

Environmental impact of tidal power in the Eastern Scheldt Storm Surge Barrier



Appendix C: CFD simulations of the Eastern Scheldt Barrier with and without tidal turbines

Prepared for:

DMEC WP3.7, Kansen voor West: UP16-00127
Deltares project: 11200119

CFD simulations of the Eastern Scheldt Barrier with and without tidal turbines

Validation study and determination of discharge coefficients

Tom O'Mahoney

11200119-003

Title

CFD simulations of the Eastern Scheldt Barrier with and without tidal turbines

Client	Project	Reference	Pages
Dutch Marine Energy Centre	11200119-003	11200119-003-HYE-0004	30

Keywords

Tidal Energy, Eastern Scheldt Barrier, CFD, Turbines

Summary

As a step to estimate the impact on energy production and environment of tidal turbines placed in the Eastern Scheldt Storm Surge Barrier a Computational Fluid Dynamics (CFD) study has been carried out to study the flow around the turbines and the effect of the turbines on the discharge through the gate. This study is part of a broader project to assess the effect of the turbines in the barrier which is described in [1].

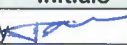
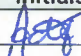
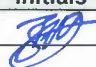
The CFD model focusses on a single gate opening of the Storm Surge Barrier and includes half of the adjoining gates on either side. In this 40 m wide Gate a 1.2 MW array existing of five Tocardo T2 tidal turbines have been installed in 2015.

Transient computations of the barrier with and without the turbine array were carried out for a range of quasi stationary tidal phases. The turbines are resolved in detail as rotating equipment with the real-time rotation of the turbine blades (involving the displacement of the mesh nodes in an unsteady setting). Based on the prescribed rotational speed of the turbine, the torque and thrust is provided as output.

Based on these computations an estimate of the effect of turbines on the discharge capacity of the storm surge barrier is given. This information will be used to parameterize the tidal turbines in the far-field hydrodynamic model of Eastern Scheldt estuary for a further assessment of the effect of tidal turbines on energy production and on the environment.

References

DMEC WP 3.7, Kansen voor West: UP16-00127
 Deltares, Environmental impact of tidal energy plant in Eastern Scheldt Storm Surge Barrier, 11200119-000-HYE-0006

Version	Date	Author	Initials	Review	Initials	Approval	Initials
	aug. 2018	Tom O'Mahoney		Anton de Fockert		Bas van Vossen	

State

final

Contents

1	Introduction	1
1.1	Background	1
1.2	Objective and approach	2
1.3	Research framework DMEC	2
2	Methodology	3
2.1	Simulation schedule	3
2.2	Numerical setup of CFD model	3
2.2.1	Software	3
2.2.2	General model settings	3
2.2.3	Geometry	4
2.2.4	Mesh	6
2.2.5	Boundary conditions	7
2.2.6	Turbines rotation rate	9
2.3	Discharge coefficients	10
2.4	Power	10
2.5	Thrust	12
2.6	Velocity profile measurements	12
3	Simulation results	14
3.1	Barrier without turbines	14
3.1.1	General flow pattern	14
3.1.2	Velocity profiles	15
3.1.3	Discharge coefficients	19
3.2	Barrier with turbines	19
3.2.1	General flow pattern	19
3.2.2	Velocity profiles	21
3.2.3	Discharge coefficients	23
3.2.4	Turbine power	24
3.2.5	Thrust	25
4	Discussion	27
4.1	Validation of the model	27
4.2	Inclusion of rotating zones around the turbines	27
4.3	Biofouling of the Eastern Scheldt Barrier	27
4.4	Inertia effects in the Eastern Scheldt	28
4.5	Possible discrepancy in velocity measurements	28
5	Conclusions	29
6	References	30
	Appendices	
A	Detailed drawings of the geometry and turbines as present in the CFD model	A-1

B Velocity profiles without turbines

B.1 Horizontal ADCP validation

B.2 Vertical ADCP validation

B-1

B-1

B-3

C Velocity profiles with turbines

C.1 Case 1 (head difference = -0.2m)

C.2 Case 2 (head difference = -0.32m)

C.3 Case 3 (head difference = +0.2m)

C.4 Case 4 (head difference = +0.55m)

C-1

C-1

C-2

C-4

C-5

1 Introduction

1.1 Background

The Eastern Scheldt Storm Surge Barrier consists of 62 individual gates, and is constructed of concrete pillars, top beams and sill beams connecting to a rockfill sill construction and about 600 m of bed protection on both sides, see [2]. During ebb and flood the maximum head difference over the barrier is about 1 m, with maximum velocities of 4 m/s and higher, making it an ideal site for the generation of tidal stream energy.

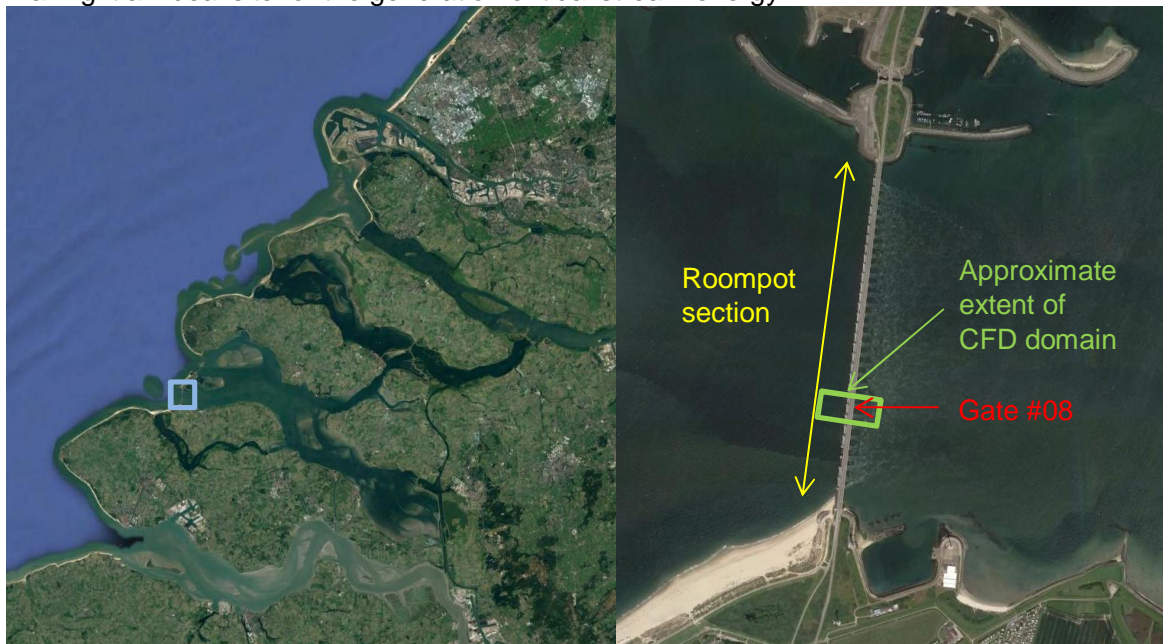


Figure 1.1 Location of Gate #08 of the Roompot section of the Eastern Scheldt Barrier, shown on a satellite image (source: Google Earth)

In 2015 an array of five tidal turbines was deployed in Gate #08 of the Roompot Section of the barrier in the framework of a tidal power pilot project. This project initiated the development of numerical modelling tools to assess the effects of the tidal turbines in this type of barrier. Previously, the CFD modelling of a tidal turbine in the proximity of the free surface was addressed, [3]. As a second step, the CFD modelling of the flow through the gates of the barrier (without turbines) was studied and compared with field measurements of ADCP horizontal and vertical profiles near the gate opening [4]. This report concerns simulations that combine both the modelling of the turbine array in combination with the structure of the Storm Surge Barrier. A comparison with field ADCP measurements is included.

Research on the flow around tidal turbines that is available in the literature has concentrated on the performance of the tidal turbines and has been conducted with BEM methods ([5, 6]), CFD with frozen rotor [7] or actuator disc [8, 9]. More recently CFD methods with rotating turbine blades in a sliding mesh configuration have been used to give a more detailed view of the flow field and turbulence at the inlet and wake of the turbines. Most experiments [10-13] consider isolated turbines at lab scale for a marine current application where the flow is unidirectional. Subsequently, CFD validation efforts have therefore mostly concentrated on such situations ([14-17]). Very few studies [18] have studied flow directionality. As the turbines in these studies are isolated the blockages are relatively low (from 6 % in [9], 12 % in [11], to 17 % in [19, 20]), although in one study a very high blockage was used [21]. Higher

blockages have also been studied for cross flow turbines [22]. However, turbines located in a Storm Surge Barrier will have a higher blockage than those available in this literature.

Similarly the location of turbines in a pre-existing hydraulic structure leads to complex inflow conditions and interactions with the structure. Some authors have shown the importance of inflow velocity profile and inflow turbulence on turbine performance, wake development and the performance of CFD models [8, 23, 24]. The interaction with other turbines in arrays, both in terms of performance and wake recovery, has been studied but only in the absence of other structures [25-28]. Similarly an uneven bathymetry is often not included although the probable importance is stressed [13]. Field measurements in a real bathymetry have been made [29], although only in the absence of turbines, and consequently lab scale measurements were scaled up for the CFD simulations with a turbine [17]. Alternatively the CFD has been performed at full-scale with measured inflow profiles [30].

1.2 Objective and approach

The aim of the current report is to combine the modelling of bathymetry, surrounding structures and rotating blades to simulate a field scale tidal turbine array with high blockage owing to its location in a Storm Surge Barrier. Comparison with field scale measurements at the location of the turbines, with and without turbines is made. The CFD results give information about the effect of the tidal turbines on the discharge coefficient of the barrier as well as the flow field downstream of the turbines.

1.3 Research framework DMEC

Dutch Marine Energy Centre (DMEC) is a consortium of 15 partners researching topics that are related to energy from water. This research is part of the DMEC project - task 3.7, which is led by Deltares. Research task 3.7 aims to use and develop tools to investigate the near field and far field hydrodynamic behaviour near the Tidal Power Plant that is located in the Eastern Scheldt Storm Surge barrier.

An analysis of the field scale experiments is given in detail in a separate report [31] and a broader view of all the aspects of research tasks 3.7 is given in [1].

2 Methodology

The CFD computations have been performed using STAR-CCM+. The flow through the barrier is simulated including the free surface. The highly detailed pillar and sill geometry result in an extremely turbulent flow downstream of the barrier and in this work an eddy-resolving turbulence model is used.

2.1 Simulation schedule

The four cases chosen for this study include two ebb cases and two flood cases, see [31]. The four cases are moments in the tidal cycle at which the ADCP data has been analysed. The range of the water levels and heads is determined by the range of ADCP data for which a positive quality check is available. They do not cover the entire range of operation of either the turbines or the wished for extension of operations of the turbines. For the CFD simulations the water levels are considered to be constant, which has the effect of excluding tidal inertia effects from the model. This is further addressed in the discussion section.

Table 2.1 Summary of the conditions for the simulations (NT represents No Turbines, WT represents: With Turbines)

	Case number	Water Level North Sea	Water Level Eastern Scheldt	Head
		t.o.v. NAP	t.o.v. NAP	[m]
Ebb	NT.1 / WT.1	0.93	1.13	-0.20
	NT.2 / WT.2	0.68	1.00	-0.32
Flood	NT.3 / WT.3	-0.57	-0.77	0.20
	NT.4 / WT.4	1.12	0.57	0.55

2.2 Numerical setup of CFD model

2.2.1 Software

The simulations have been performed using the Star-CCM+® software, version 11.02.10, a proprietary and commercial CFD package. Star-CCM+ is able to solve the Navier-Stokes equations for mass and momentum in a three-dimensional domain, both steady-state or transient. The package also includes its own meshing algorithm. Different types of boundary conditions, numerical schemes and turbulence models are available.

Star-CCM+ has been used successfully by Deltares in recent years for the simulation of free surface flow in and around hydraulic structures, e.g. shipping locks and sluices, sewage systems and tidal energy applications. Previous validation of flows around tidal turbines [3] and the Eastern Scheldt Barrier [4] have also been performed with this software.

2.2.2 General model settings

The equations are solved in transient form, with 1st order temporal discretization, and a segregated pressure-based solver. The equations are discretized on a structured 3D grid. The Finite Volume method is used with 3rd order combination of MUSCL and Central Difference for the discretisation of the advection terms. To model turbulence near the turbines and near the sill of the barrier, Improved Delayed Detached Eddy Simulation (IDDES) turbulence model has been applied. This model uses a Large-Eddy Simulation approach in the bulk flow and a Reynolds-Averaged Navier Stokes approach in the near wall region. The near wall model uses the SST k-Omega model with wall functions. Figure 2.1 shows the

regions in which each model type is applied; a LES model is used for the vast majority of the domain (blue region in the figure). To model the free surface air and water are included as immiscible phases in the Volume of Fluid (VOF) model. A time step of 0.05 seconds is used for the final simulations although some of the spin-up of the simulations is performed with a higher time step 0.1-0.5 s. In all cases the time step and mesh are sufficient to achieve a sharp interface for the volume fraction of water between air and water, this interface being no more than 1 or 2 cells in the vertical at all locations.

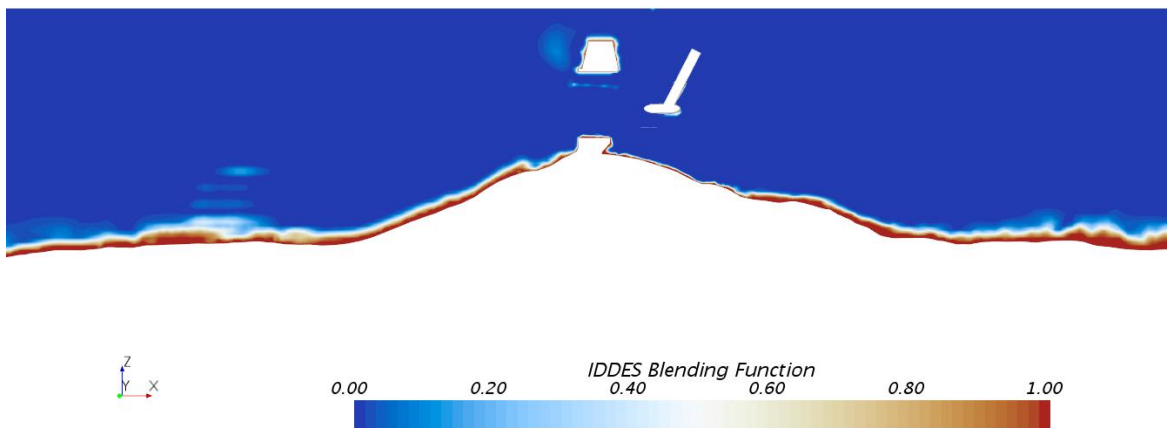


Figure 2.1 Vertical cross section of the domain showing, via the IDDES blending function, the regions where LES is performed (in blue) and those where RANS is performed (in red)

2.2.3 Geometry

The geometry of the CFD simulations encompasses a region approximately 200 m upstream and 200 m downstream of the barrier. The bathymetry has been generated from multibeam data (resolution 0.5 m) of the Eastern Scheldt region of 2017 provided by Rijkswaterstaat and converted to an stl file, with a resolution of 2 m. It is integrated with the 3D CAD of the barrier and the turbines (provided by Tocardo).



Figure 2.2 Contour plot of the bed elevation. Dimensions are with reference to NAP

The geometry encompasses one full port of the storm surge barrier (Roompot 8) and half of the neighbouring ports on each side. The geometry has been updated and verified based on the as built drawings from Rijkswaterstaat and photographs of the structure during

installation. A detailed overview of the storm surge barrier, the bathymetry and the turbines is presented in Appendix A.

The bathymetry bed levels can be seen in Figure 2.2. The extent of the bed protection is visible on either side of the barrier where the variation in the breadth is limited. Away from the bed protection the depth variations at the same distance from the barrier can be as much as 3 m in the breadth.

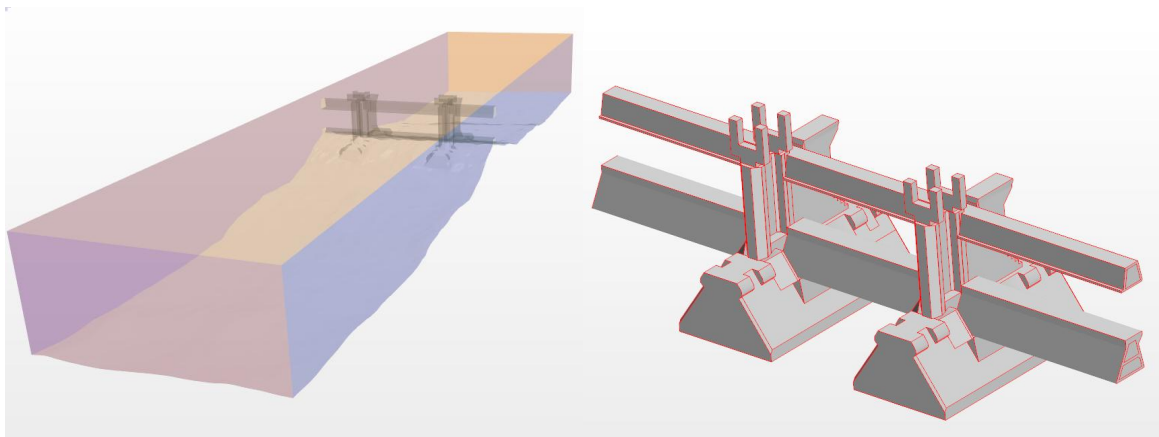


Figure 2.3 3D view of the CFD domain (left) and of the barrier CAD before integration with the bathymetry data (right) – both seen from the North Sea

The turbine geometry has been provided by Tocardo, the manufacturer and operator of the turbines. The turbine has two blades and is mounted on a support from above. There are 5 turbines in the port of Roompot 8, each with a diameter of 5.2 m. The distance between the axes of each turbine is 6.7 m. The configuration can be seen in Figure 2.4 with all turbine blades in the same orientation. In the simulations the turbines do not rotate in sync but at different (but constant) rotating speeds from each other (see also Section 2.2.6). After some spin-up time the turbines are at very different orientations from each other at any given time. A rotating zone made of a cylinder of 6 m diameter and 3.2 m length is located around each turbine hub. Ideally a larger rotating zone should be used for CFD calculations so that the interpolation between the rotating zone and the stationary zone (occurring at the interaction surface between the two zones at each time step) is performed at a location where the gradients of the flow are small and the numerical errors in interpolation have a small effect. However, for these simulations the rotating zone around the turbines is limited in size owing to the requirement that they don't overlap with each other or have a very small gap between them where cell quality would be low. A zone of 6 m diameter has been used because it allows for good quality cells between the different rotating zones and is therefore considered acceptable for this study.

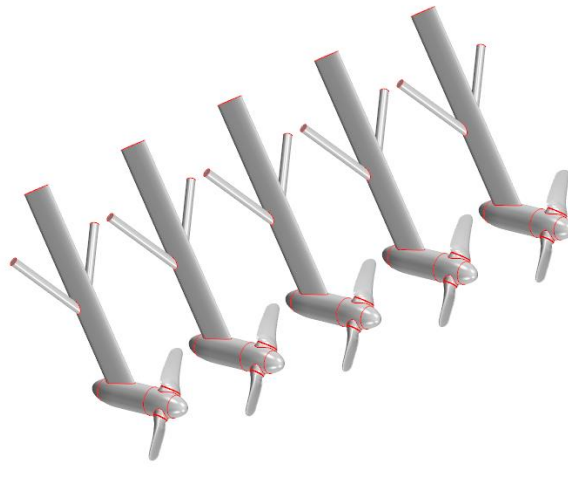



Figure 2.4 3D CAD view of the five turbines with support structure

2.2.4 Mesh

The mesh has been generated in Star-CCM+ using multiple areas of mesh refinement (see Figure 2.5). The largest cells in the domain are in the far field near the boundaries and are cube cells of size 1.2 m. Given that the water depth is approximately 30 m in this region, this gives a minimum of 20 cells in the vertical. The mesh is refined in the region 60 m upstream and downstream of the barrier such that the cells in this region become slightly elongated with the longitudinal and transverse dimension still 1.2 m, but with vertical dimension 60 cm. The water depth in this region can be as low as 18 m but still this mesh gives approximately 30 cells in the vertical. Around the barrier sill itself the cells are refined further and are again cubic with dimension 16 cm. The height of the opening above the sill is approximately 10.5 m but the water depth can be 9 m. In any case the mesh has at least 40 cells in the vertical.

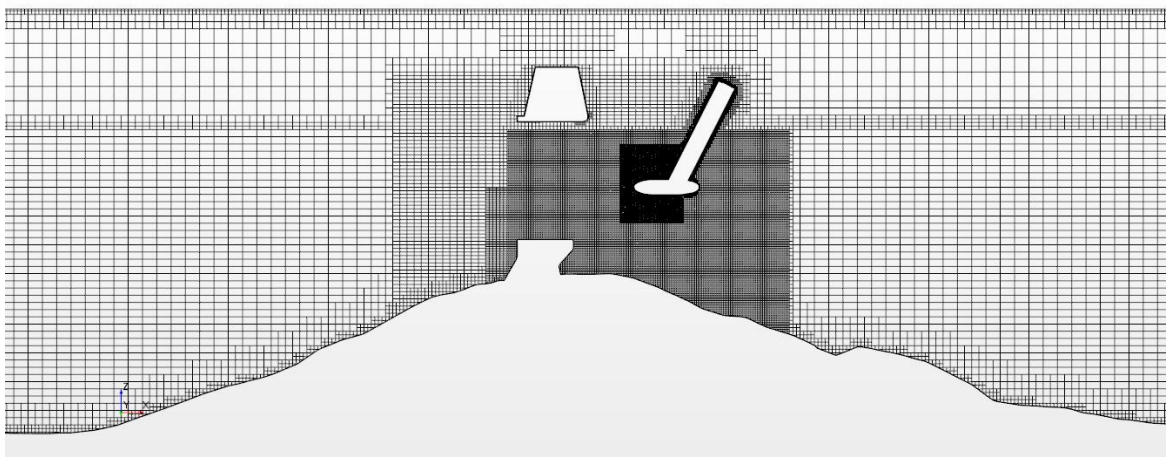



Figure 2.5 Detail of the mesh refinement zones around the sill of the barrier

In the cases where the turbines are included the mesh in the turbine wake is refined to 32 cm and in the rotating zone around the turbine is further refined to give a cell size of 8 cm but even more refinement is added at the turbine itself in order to better model the boundary layers at the surface (see Figure 2.6).

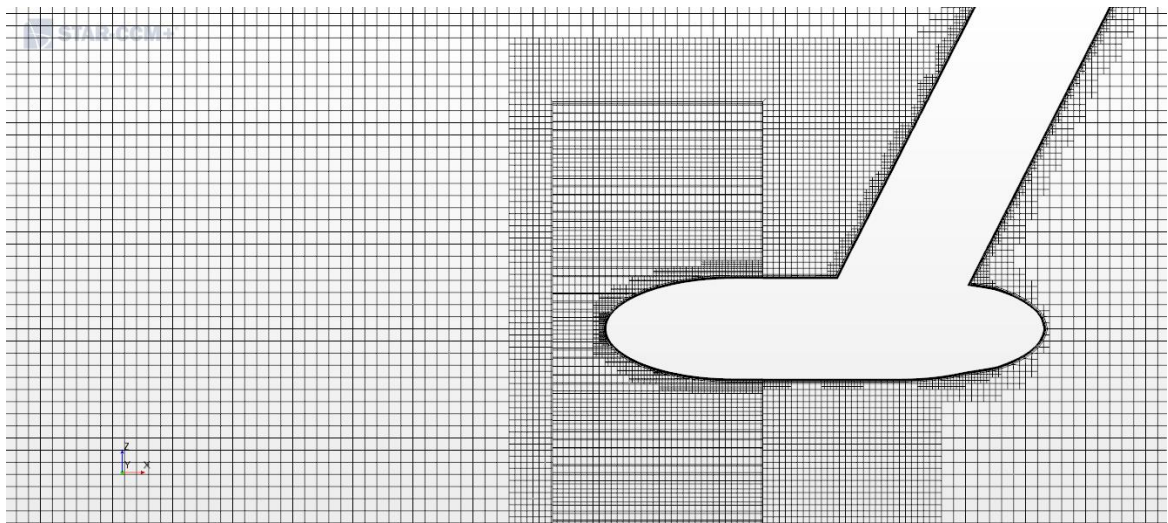


Figure 2.6 Detail of the mesh refinement zone around the turbine

Similarly in all simulations (with and without turbines) an inflation layer is added to the walls of the barrier and at the bed of the domain where the bathymetry of the Eastern Scheldt and North Sea has been included. The first cell next to the wall or bed is of the order of 3 mm in this region. This value has been chosen to achieve the correct y^+ value for the application of wall functions (see Figure 2.7). The expansion rate away from the wall or bed is high (the first cell outside of the prism layer can be as much as 5 times the prism layer thickness) to reduce the total computational effort. This parameter was varied in the mesh dependence studies and shown to have no effect on the area of interest.

STAR-CCM+

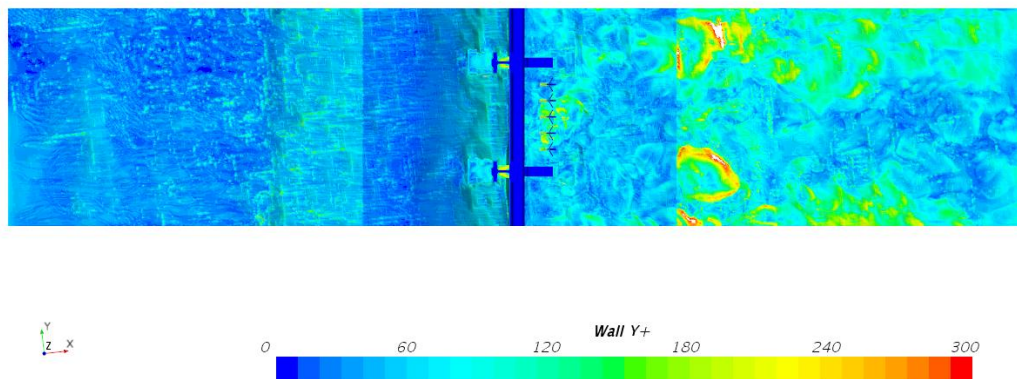


Figure 2.7 Contour plot of the wall y^+ value on the bed

2.2.5 Boundary conditions

The boundary conditions are combination of water levels and inlet velocity along with no-slip boundaries for the wall boundaries at the barrier and bed. The conditions at the inlet and outlet boundaries are constant throughout the simulation giving a flow field without inertial effects associated with a varying tidal water level.

The location and names of the boundaries are shown in Figure 2.8. Water levels are set at the downstream boundaries with a profile of the volume fraction of water, where the volume

fraction is 1 below the water level and 0 above it. The downstream boundary is the Eastern Scheldt for flood cases and the North Sea for Ebb cases. An initial water level is also set for the upstream boundary in the same way along with a velocity profile. This initial water level may not be consistent with the discharge through the barrier and the downstream water level and therefore the upstream water level varies during the simulation. In order to have results for the desired set of conditions in Table 2.1, the velocity profile is scaled to adjust the discharge until the achieved upstream water level is within 1 cm of the desired level. This water level is always averaged over the breadth of the domain and then time-averaged.

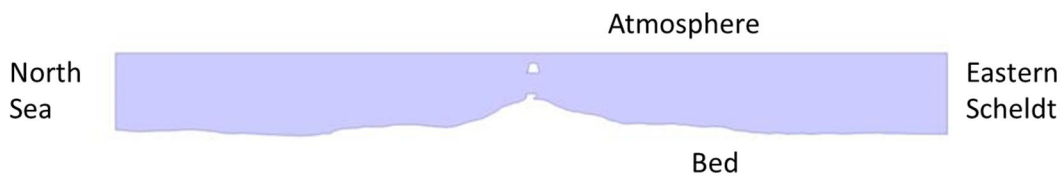


Figure 2.8 Vertical cross section of the domain showing the names of the boundaries

The barrier itself includes the sill and the pillars which are of concrete. They are modelled as no-slip walls with a roughness of worn concrete (1 cm). The bed of includes the small scale variations of the bed protection and seabed and has been modelled as a no-slip wall without additional roughness. The sides of the domain located at the halfway point between the two pillars in gate 7 and 9 so that a symmetry boundary condition can be used.

Table 2.2 Summary of the boundary conditions used in the simulations

Boundary	Condition
North Sea / Eastern Scheldt	Inflow profile and water level
Bed	No-slip wall (smooth – no roughness)
Barrier	No-slip wall with roughness
Atmosphere	Atmospheric pressure
Sides	Symmetry

2.2.5.1 Inflow velocity profile

ADCP data of the velocity profile in the Eastern Scheldt is available for a number of measurement points. MP0002 is in the Eastern Scheldt 750 m from the barrier and at a location where the bathymetry is representative for the inflow conditions to Roompot 8. A comparison of measured velocity profiles in the Eastern Scheldt shows that a logarithmic profile is representative.

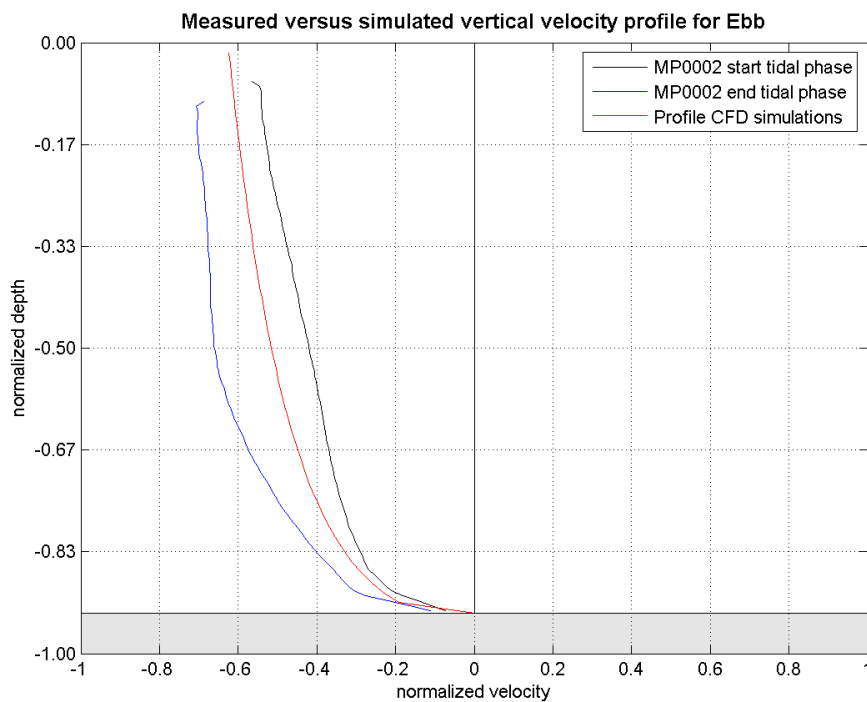


Figure 2.9 Measured profile at MP0002 (750m before barrier at Eastern Scheldt side) versus logarithmic vertical profile used in CFD

Figure 2.9 shows comparison of the measured profile during Ebb which would be representative of the inflow condition for the CFD model, along with an example of the logarithmic profile used for the CFD (scaled to the depth at that location). The measurements show a variation in the profile between the start of the tidal phase and the end of the tidal phase. The CFD profile is between these two measured profiles and is therefore a good model of the average inflow conditions at the barrier.

2.2.6 Turbines rotation rate

The rotation speed of the turbines is applied to the model as an input parameter. The rotation speeds are based on measured RPMs at the turbines. For each turbine a median is made over a number of tidal cycles of the RPM at each head to give a relation between the head difference and the median RPM (shown in Figure 2.10 for turbine T12-1). The rotation speed in the simulations is therefore chosen to correspond to the head difference of the simulation; a different speed is therefore given to each turbine (for more information see [31]). A summary of the rotation speeds used in the simulations is given in Table 2.3.

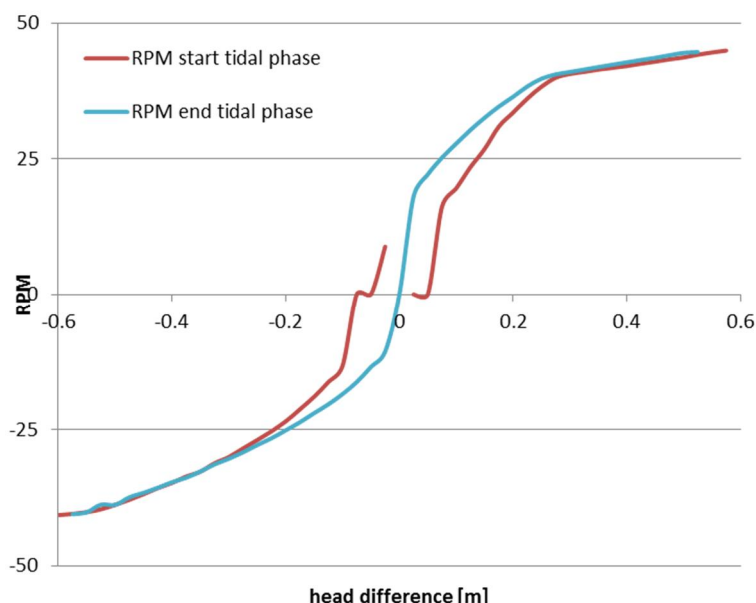


Figure 2.10 Example plot of the dependence of the turbine RPM on head difference

Table 2.3 Summary of the rotation rates for the turbines

	Case number	T12-1	T14-2	T11-3	T15-4	T09-5
		[rpm]	[rpm]	[rpm]	[rpm]	[rpm]
Ebb	WT.1	0.93	-24.33	-24.03	-23.03	-23.66
	WT.2	0.68	-31.29	-31.17	-30.52	-30.97
Flood	WT.3	-0.57	34.95	35.42	34.50	35.07
	WT.4	1.12	44.57	44.86	44.47	44.61

2.3 Discharge coefficients

The discharge through the barrier depends on resistance of the barrier and the head across the barrier. A non-dimensional coefficient, the discharge coefficient gives the relation between the head and the discharge for a given situation. It is dependent on the cross section: in case of the Eastern Scheldt barrier this is also dependent on the water level. The discharge can be described by the following formula.

$$Q = \mu A \sqrt{2g\Delta h}$$

In which Q is discharge [m³/s], μ discharge coefficient [-], A the wetted cross-sectional area in the poort, [m²], g gravitational constant [m/s²] and Δh water level difference [m].

2.4 Power

The generated power of the turbines has been analysed in a similar way to that of the rotation rates; giving a median power over many tidal cycles as function of the head difference (see also [31]). The resulting power for the head differences in each of the simulation conditions is given in Table 2.4. The power generated in the simulations is not specified but is a result of the simulation. The moment and force on the turbines is a direct output from the simulations, calculated by Star-CCM+ as an integration of pressure across the surface of the blades. The information of the measured power is used for comparison with the CFD in the results section. The values as specified in Table 2.4 are measured power values to the grid. Due to

energy losses, the power to the rotor is about 10% higher. This is further discussed in Section 3.2.4.

Table 2.4 Summary of the measured power of the turbines

	Case number	T12-1	T14-2	T11-3	T15-4	T09-5
		[kW]	[kW]	[kW]	[kW]	[kW]
Ebb	WT.1	13.76	12.73	11.27	12.28	9.85
	WT.2	32.57	31.10	29.73	31.04	29.31
Flood	WT.3	46.26	46.80	43.93	45.97	46.79
	WT.4	191.01	193.87	186.00	188.73	192.77

For case WT.1, turbine 5 has a lower power value than the other 4 turbines. By investigating this further, it was seen that the power that is generated at the start of the tidal phase is significantly lower than at the end of the tidal phase. This is most likely the result of the approach flow towards the turbines, which is straighter at the end of the tidal phase than during the start of the tidal phase (see Figure 2.11). This figure is based on Delft3D numerical model results at 200 m upstream of the barrier ([32]). This means that for ebb (red dots), the approach flow velocities at 200 m from the barrier in the North Sea are analysed and during flood (blue dots), the approach flow velocities at 200 m from the barrier in Eastern Scheldt are analysed. In this figure it is seen that for lower flow velocities (up to 0.5 m/s) during ebb, the angle can be either 31° or 6° with respect to the barrier. The larger angle represents the start of the tidal phase and the more straight approach flow represents the end of the tidal phase. An oblique approach flow leads to a reduced power production, particularly in turbine 5.

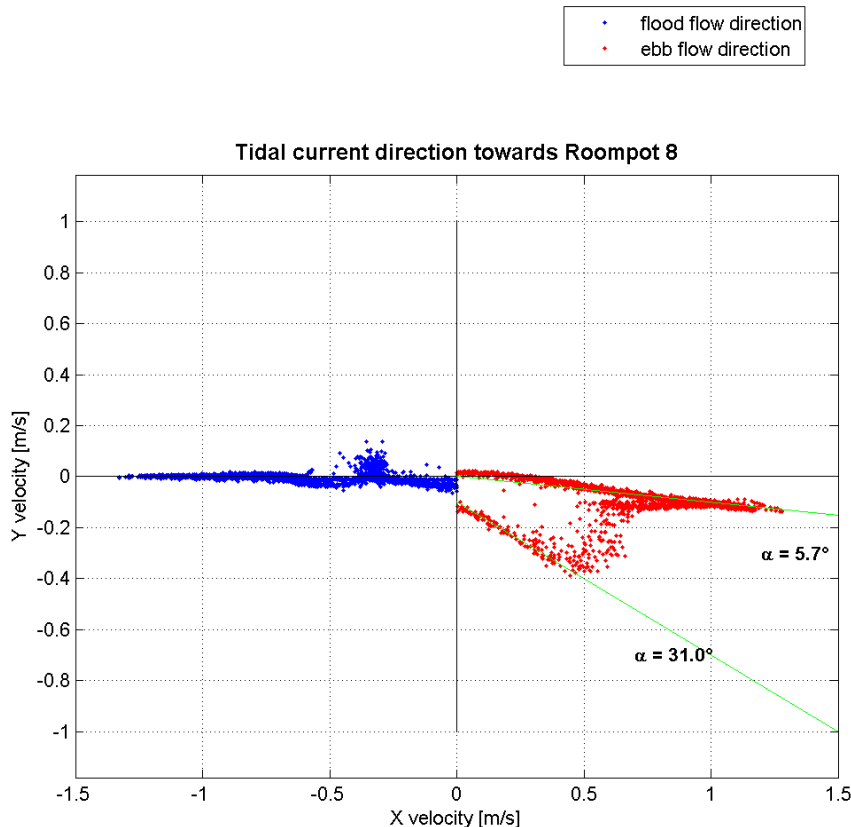


Figure 2.11 Approach flow angle towards gate 8 of the storm surge barrier. The red dots represent ebb and show the approach flow angle towards the barrier. The blue arrows show the approach flow angle towards the barrier during flood

2.5 Thrust

Thrust measurements have been performed by Tocardo on the 3th and 5th turbine in the barrier. Similar to the power measurements, these measurements have been analysed and used as validation by the CFD model. The thrust is measured with thrust gauges, which are mounted on the strut of the turbine. The values as presented in Table 2.5 are analysed based on the head differences over the barrier, similar to the power and ADCP measurements (see also [31]).

Table 2.5 Summary of the measured thrust on the turbines

	Case number	T12-1	T14-2	T11-3	T15-4	T09-5
		[kN]	[kN]	[kN]	[kN]	[kN]
Ebb	WT.1	n/a	n/a	-20.00	n/a	-25.43
	WT.2	n/a	n/a	-33.97	n/a	-40.06
Flood	WT.3	n/a	n/a	43.25	n/a	45.39
	WT.4	n/a	n/a	105.04	n/a	117.68

2.6 Velocity profile measurements

ADCP measurements have been carried for both the situation before turbine deployment (2011) and during turbine deployment (2016, 2017). Only the location of the measurements are mentioned here as further analysis of the measurements has been made in [31].

Figure 2.12 shows the locations of the horizontal and vertical ADCP measurements that have been carried out in 2011 before the turbines were installed in Gate #08. Both ADCP devices were installed at the Eastern Scheldt side of the sill beam. The measurements were carried out for a period of 6 days.

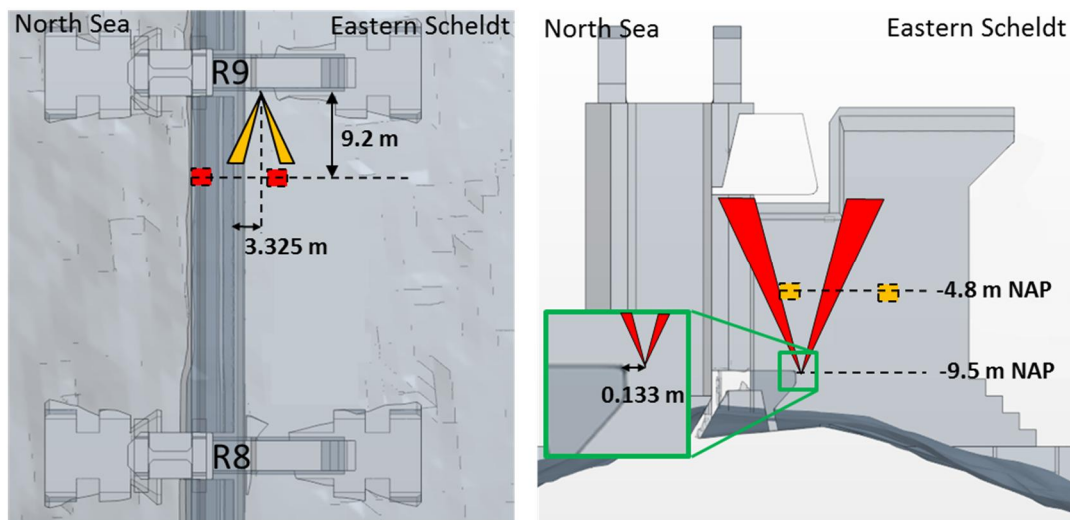


Figure 2.12 Overview of the 2011 ADCP measurements. Left: Top view, right: Side view.

In 2015, 5 turbines were installed on the Eastern Scheldt side of Gate #08 of the Eastern Scheldt Barrier Roompot section. The middle and outer turbines were equipped with two ADCP's, one pointed forwards (towards the North Sea) and one pointed backwards (towards the Eastern Scheldt), see Figure 2.13. The ADCP devices measure along 1 beam by default, but have also been used to perform 5-beam measurements. Different periods have been measured. These periods are listed in Table 2.6.

Table 2.6 ADCP measurement periods with and without turbines

Measuring period		Turbine operation	Signal
15/08/2011 – 21/08/2011	6 days	No turbines	Horizontal + vertical ADCP
10/10/2016 – 26/10/2016	14 days	Normal operation	1 beam
22/06/2017 – 24/06/2017	1 day	Normal operation	5 beams
28/08/2017 – 29/08/2017	1 day	Stall mode	1 beam
14/09/2017 – 15/09/2017	1,5 day	Stall mode	5 beams

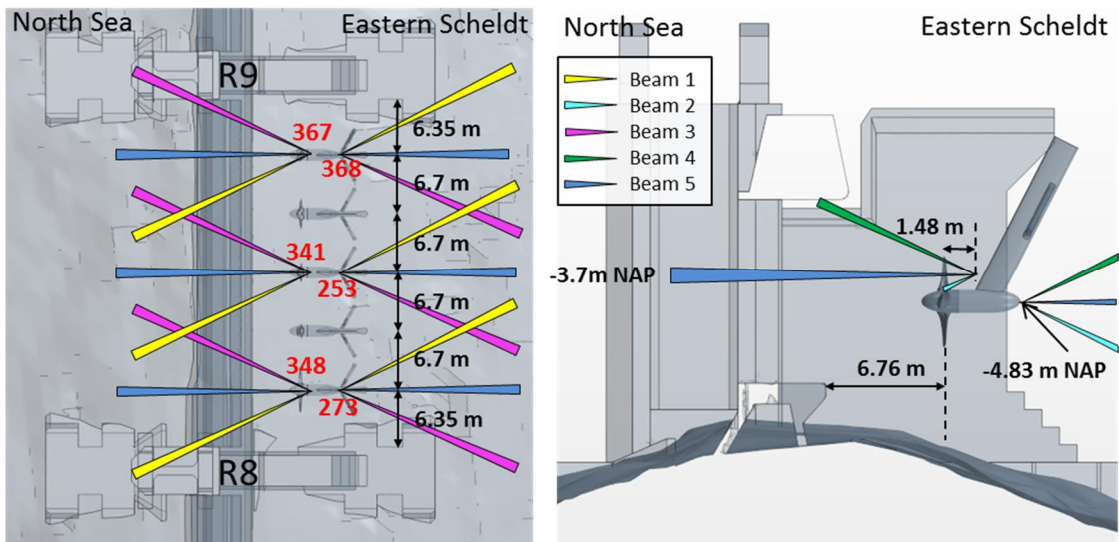


Figure 2.13 Top view (left) and side view (right) of the turbine configuration at Gate #08 of the Eastern Scheldt Roompot Section. The red numbers show the names of the forward-looking and backward-looking ADCP devices.

3 Simulation results

3.1 Barrier without turbines

3.1.1 General flow pattern

The flow pattern shows an acceleration of the flow towards the barrier because of the decrease in water depth. A large flow separation occurs at the upstream edge of the sill of the barrier (see Figure 3.1). This separation creates a recirculation zone downstream of the barrier where the dominate flow direction is back towards the barrier. The flow reattaches to the bed at approximately 100 m downstream (not shown in the figure). In addition the separation causes concentration of the flow at the surface such that the maximum velocity of the flow is some distance downstream of the barrier opening rather than in the opening itself.

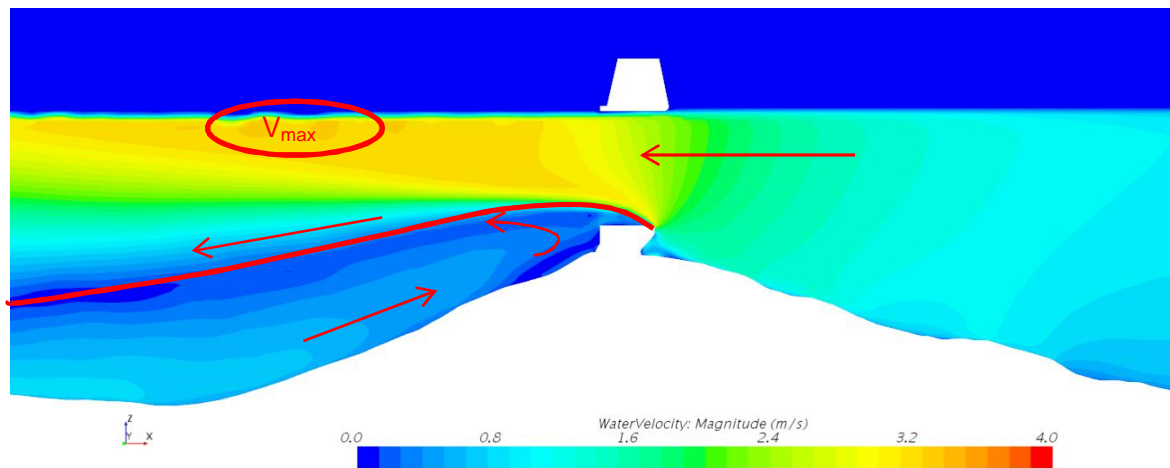


Figure 3.1 Contour plot of mean velocity magnitude on a vertical cross section from case NT.2; an ebb case with a detail of the flow around the sill. The recirculation zone is shown by a red line and the direction of flow is given by a red arrow.

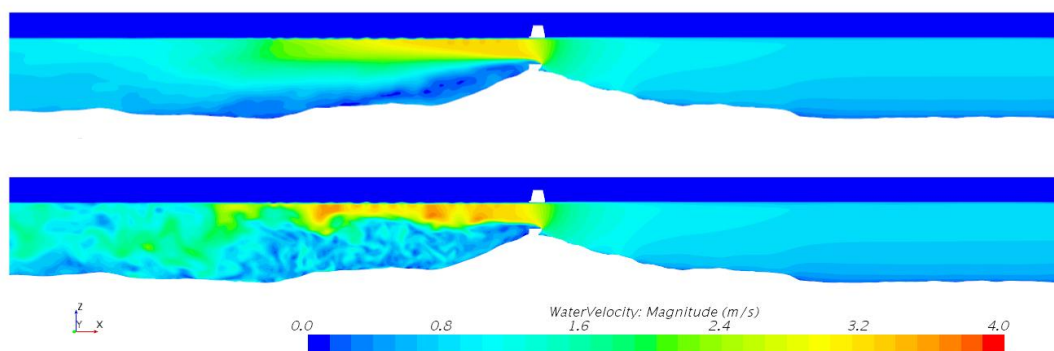


Figure 3.2 Contour plot of velocity magnitude on a vertical cross section from case NT.2; an ebb case

Figure 3.2 shows the flow field for an ebb case where the flow is from right (Eastern Scheldt) to left (North Sea). A comparison is shown between the mean field (top) resulting from an average over a long time (a number of minutes) and the instantaneous field which is the result of each time step. The large scale eddies resulting from the vortex shedding occurring

at the barrier are visible in the instantaneous plot but these are averaged out in the mean field. Many scales of eddies, as small as approximately a couple of cell sizes, can be resolved with the DES model.

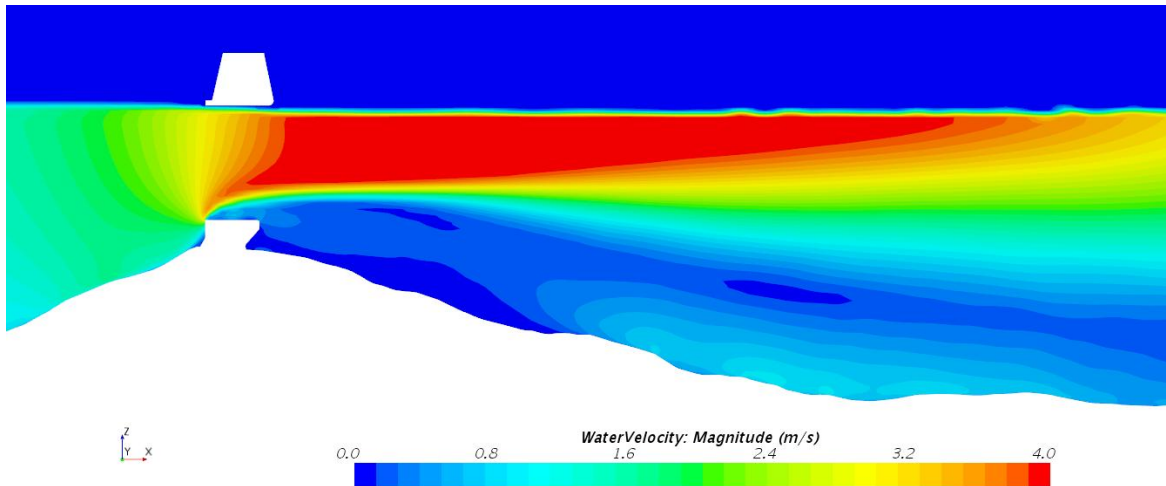


Figure 3.3 Contour plot of mean velocity magnitude on a vertical cross section from case NT.4; a flood case with a detail of the flow around the sill.

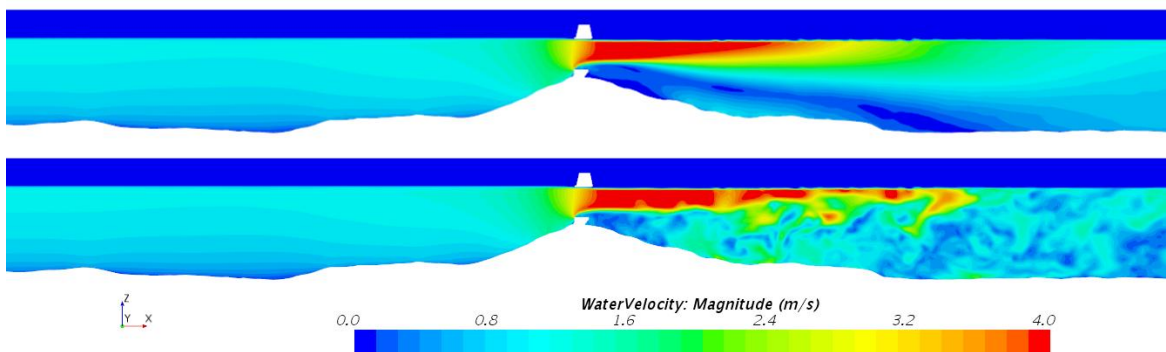


Figure 3.4 Contour plot of velocity magnitude on a vertical cross section from case NT.4; a flood case

Figure 3.3 shows a detail of the velocity contours near the sill for a flood case. Figure 3.4 shows the corresponding plots for a flood case where the qualitative flow pattern is the same but the flow is from left (North Sea) to right (Eastern Scheldt). Again flow separation occurs at the upstream edge of the barrier sill. Note that the contraction of the flow continues downstream of the sill whereby the maximum velocity is present not at the smallest cross-section (the barrier port) but downstream (the point of maximum contraction).

3.1.2 Velocity profiles

The ADCP measuring devices for the vertical profiles were mounted on the Eastern Scheldt face of the barrier sill. In the Ebb case this is in a location upstream of the point of flow separation. The vertical velocity profile (Figure 3.5) shows therefore simply an approximately logarithmic profile with a clear boundary layer starting from the height of the top of the sill. The measurements are split between a profile from the start of the tidal phase and that from the end of the tidal phase. The difference between the two profiles is due to inertia in the Eastern Scheldt (for more information see [31]). The CFD simulations are made with constant boundary conditions (water levels) and the results are taken once the flow field has reached

an equilibrium (a statistically steady state), this means that the CFD results are free from inertia. It is therefore expected that the CFD profile should fall between the two measured profiles. For this vertical profile of the ebb case NT.1 this is the case. The agreement with the numerical model is therefore considered good.

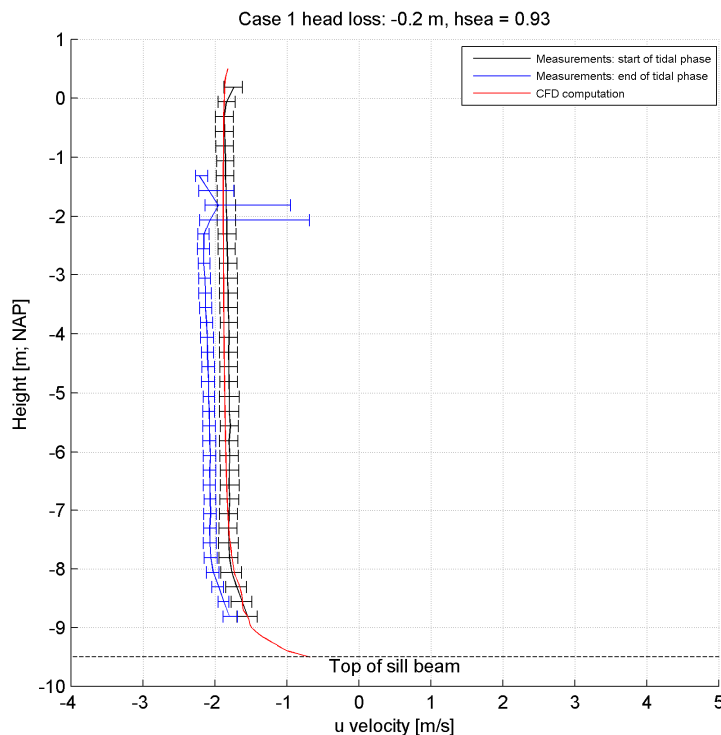


Figure 3.5 Vertical ADCP profile from the measurements without turbines – comparison between CFD and measurements – Ebb Case NT.1

The horizontal profile (Figure 3.6) shows some discrepancy in the region close to the pillar (R9) where the measured profile, which does not measure right up to the pillar, does not show any boundary layer, whereas the CFD predicts that the width of the boundary layer is penetrating into the measured zone. This could be attributed to a large roughness used in the simulations (1 cm) which may be appropriate for the sill but for the side pillars it may be too high. The velocity in the bulk of the flow is predicted to be at the correct level, as the region of the boundary layer is a negligible part of the total width of the port. This small discrepancy is not expected to result in inaccuracy in the discharge coefficient. The agreement is therefore considered acceptable.

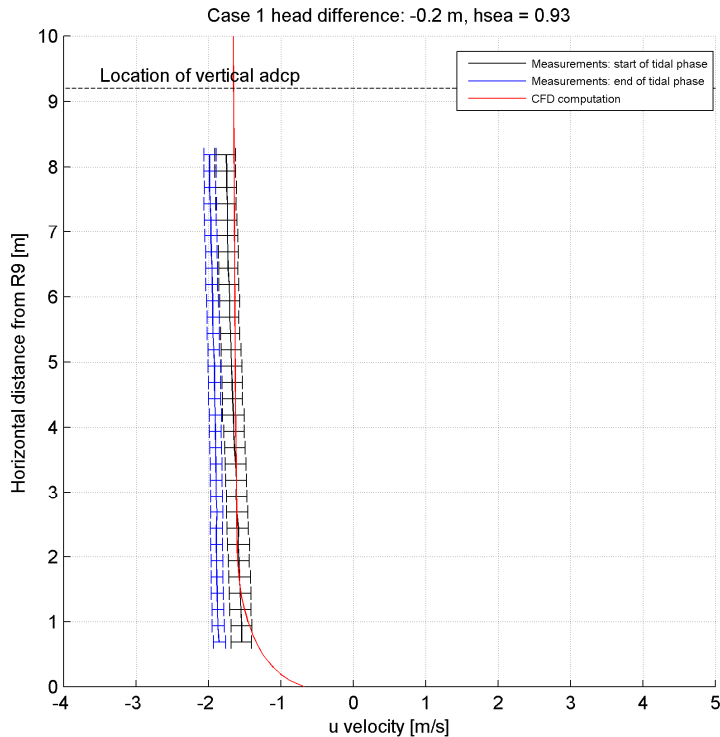


Figure 3.6 Horizontal ADCP profile from the measurements without turbines – comparison between CFD and measurements – Ebb Case NT.1

In the flood case the ADCP is located downstream of the sill and therefore is located in the recirculation zone. The comparison of the CFD results with the measurements is shown in Figure 3.7. In this case the variation between the start of the tidal phase and the end of the tidal phase in the measurements is small and the velocity in the bulk of the flow is predicted very well by the CFD model. The size of the recirculation zone is slightly larger in the CFD than in the measurements. The horizontal flow profile (shown in Figure 3.8) has similar characteristics to that in the ebb case and the agreement with CFD is equally good. The velocity profiles for the remaining cases (NT.2 and NT.3) are presented in Appendix B.

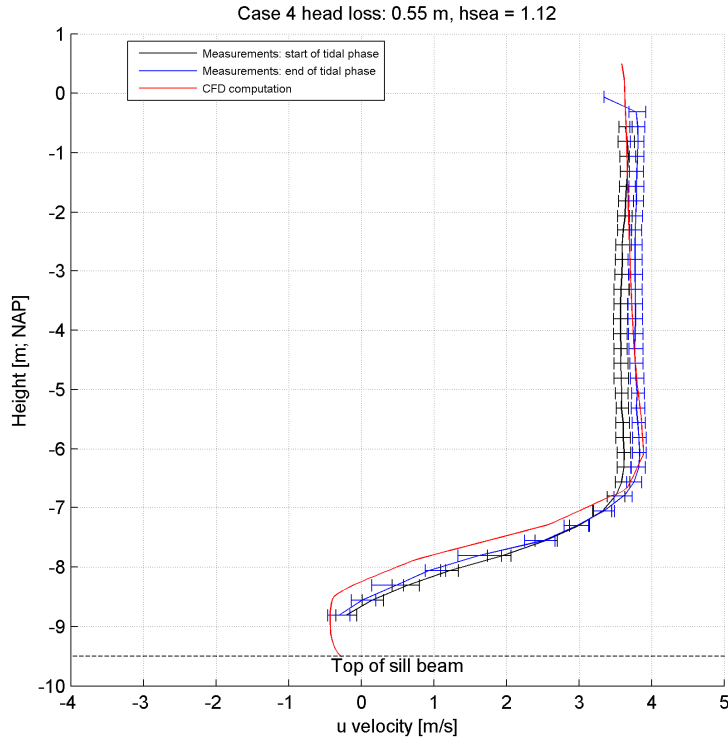


Figure 3.7 Vertical ADCP profile from the measurements without turbines – comparison between CFD and measurements – Flood Case NT.4

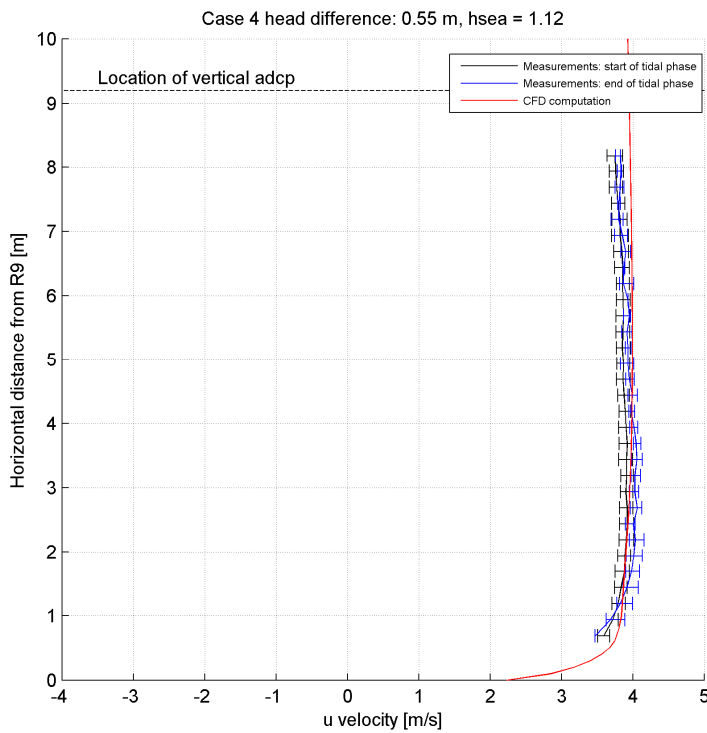


Figure 3.8 Horizontal ADCP profile from the measurements without turbines – comparison between CFD and measurements – Flood Case NT.4

The results presented in this section have been achieved after a long validation process in which the dependence of the results has been tested for many parameters. The model settings used for the definitive results produce the best results and used parameters which can be well supported from physical considerations. In particular, the use of an appropriate inflow velocity profile as a boundary condition at the edge of the CFD domain was important in producing the good match seen here. Similarly mesh resolution and quality at the edge of the sill where detachment occurs is also important.

3.1.3 Discharge coefficients

The discharge coefficients from the simulations, as defined in Section 2.3, were calculated for each CFD case. A distinction is made for a coefficient over the whole domain and between each port of the barrier. For the simulations without turbines these should be identical because of the symmetry in the geometry and boundary conditions. The discharges for the whole domain are calculated at the boundary. The Star-CCM+ monitors give a constant discharge at the inlet boundary, owing to the specification of the inlet profile there. The discharge at the outlet boundary varies during the simulation owing to the unsteadiness of the flow. The value reported in Table 3.1 is based on the value at the inlet. The discharges for the flow through the port and sides are based on a monitor of a vertical cross-section at the barrier. This type of internal monitor uses interpolation of the flow field onto the predefined cross-section which introduces small numerical errors. This is the reason why the discharge in the table for the port and sides does not sum to exactly that through the entire domain.

Table 3.1 Summary of the results for discharge coefficients for the simulations

	Case	Water Level [m NAP]		Head [m]	Discharge			μ		
		North Sea	Eastern Scheldt		Domain	Port	Side	Domain	Port	Side
				[m ³ /s]	[m ³ /s]	[m ³ /s]	[-]	[-]	[-]	
Ebb	NT.1	0.93	1.13	-0.20	1588	780	799	0.98	0.96	0.98
	NT.2	0.68	1.01	-0.33	1992	992	1009	0.98	0.98	0.99
Flood	NT.3	-0.57	-0.77	0.20	1178	582	592	0.87	0.86	0.87
	NT.4	1.12	0.58	0.55	2327	1145	1156	0.90	0.88	0.89

For the ebb cases the discharge coefficient (μ) is almost identical for each case. This can be attributed to the very similar water levels upstream in each case (the difference is only 12 cm). A discharge coefficient of 0.98 is calculated for ebb, with a head difference from 200 m upstream and downstream of the barrier. For the flood cases a discharge coefficient between the simulations between 0.90 and 0.87 is noted. For the flood cases the upstream water level varies between the cases by 1.69 m. For a barrier of this type with a lintel support which is submerged in water for the higher water levels the discharge coefficient is expected to be dependent on water levels as well as geometry.

3.2 Barrier with turbines

3.2.1 General flow pattern

For the simulations with turbines the general flow pattern is very similar (see Figure 3.9 - Figure 3.12). The turbines offer however some resistance to the flow. For the Ebb case this is hardly visible in the contour plots but for Flood cases it is clear that the contraction of the flow above the sill does not develop as strongly as in the scenario without turbines. The point of maximum velocity is therefore much closer to the sill and is located as flow is diverted around the turbines. Some of this diverted flow is directed downwards to the area below the turbines. This can be seen more clearly in a plot of the difference in velocity between the simulations

with and without turbines (shown for a flood case in Figure 3.13). Behind the turbine is an area (in blue in the figure) where the velocity with turbines is much smaller than without turbines because this is in the wake of the turbine. Below the turbine is an area (in red in the figure) where the velocity with turbines is higher than without turbines. Some of the flow is being diverted below the turbines, leading to larger velocities there. The recirculation area appears therefore smaller than for the case without turbines, but again only in the flood case.

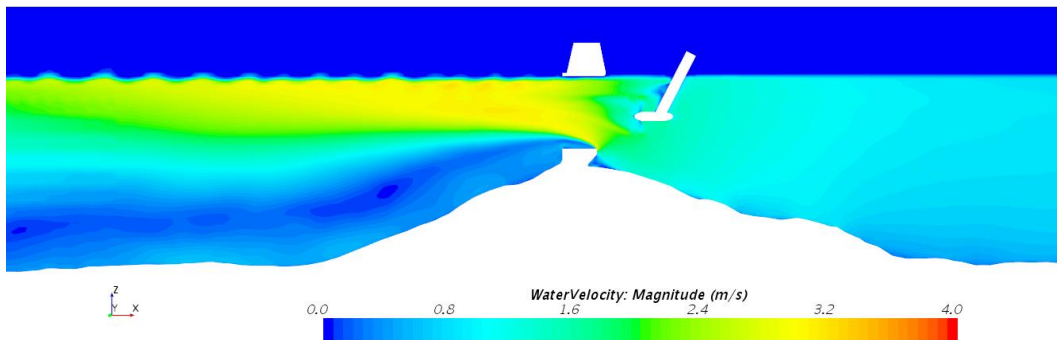


Figure 3.9 Contour plot of mean velocity magnitude on a vertical cross section from case WT.2; an ebb case with a detail of the flow around the sill.

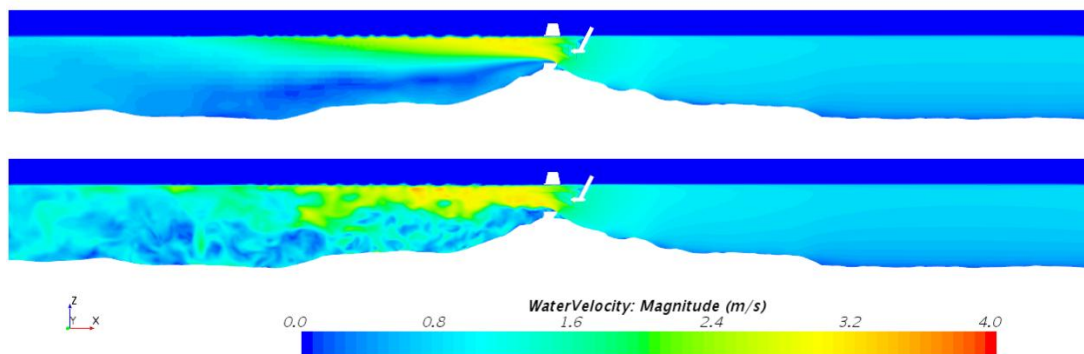


Figure 3.10 Contour plot of velocity magnitude on a vertical cross section from case WT.2; an ebb case

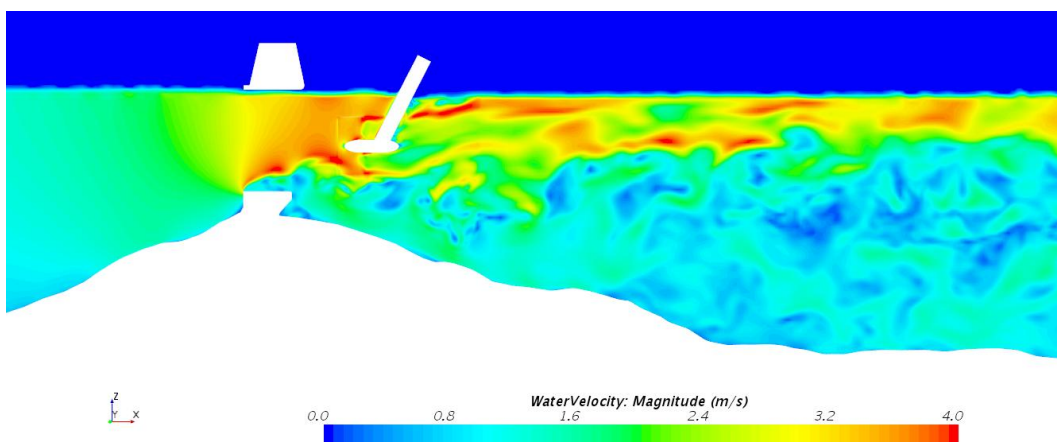


Figure 3.11 Contour plot of velocity magnitude on a vertical cross section from case WT.4; a flood case with a detail of the flow around the sill.

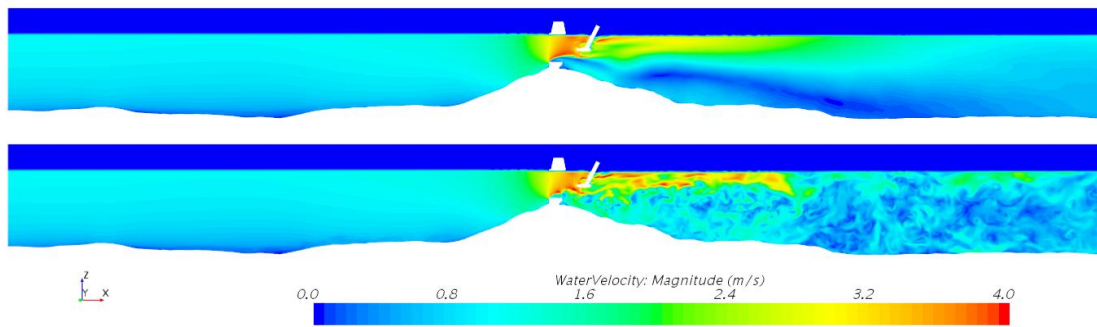


Figure 3.12 Contour plot of velocity magnitude on a vertical cross section from case WT.4; a flood case

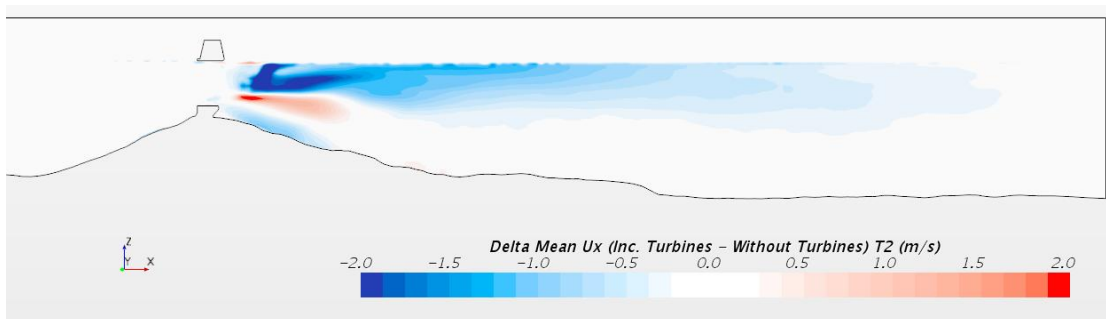


Figure 3.13 Contour plot of the difference in longitudinal velocity on a vertical cross section from case WT.4; a flood case

3.2.2 Velocity profiles

For the field measurements in the presence of the turbines the ADCP measurements were made from a device mounted on the turbines' hub and turbine support (see Figure 3.14). The main direction of the ADCP is in the longitudinal direction, or parallel with the dominant flow direction. Figure 3.15 and Figure 3.16 show the comparison of the measured profiles with the CFD simulations for respectively an ebb case (WT.1) and a flood case (WT.4). The corresponding profile of the simulation with the same conditions but without turbines is also included in the figure, this helps to give insight into the effect of the turbine on the profile.

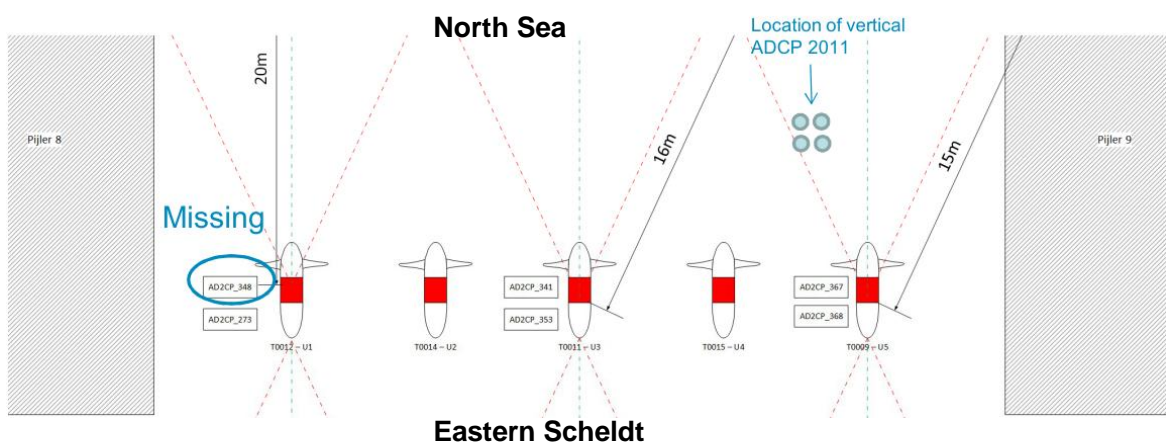


Figure 3.14 Orientation of ADCP's on the turbines

For the ebb case (Figure 3.15) the inflow profile is at the top of the figure. This shows a region of rising speed (because of the coordinate system used the velocity here is negative and

becomes more negative as it accelerates towards the barrier). The turbines are located upstream of the barrier so the velocity magnitude drops in front of the barrier in the wake of the turbines. Note that for the simulation without the turbines the flow accelerates all the way to the sill and beyond, owing to the contraction of the flow which continues downstream of the sill in that case. Downstream of the turbines the velocity recovers. The agreement with the measurements is good although downstream of the turbines the uncertainty in the measurements is large. Upstream of the turbines the CFD simulations show a small underestimation of the velocity. Also the CFD simulation with turbines shows lower velocity magnitudes than the simulation without turbines. This is owing to the difference in discharges in the two simulations owing to the extra resistance of the turbines (the profile is insensitive to the exact location in the vertical at which it is made). A slight underestimation of the velocity magnitude in the CFD when compared to the measurements could also suggest that the discharge is underestimated by the CFD. This is discussed further in Section 4.5.

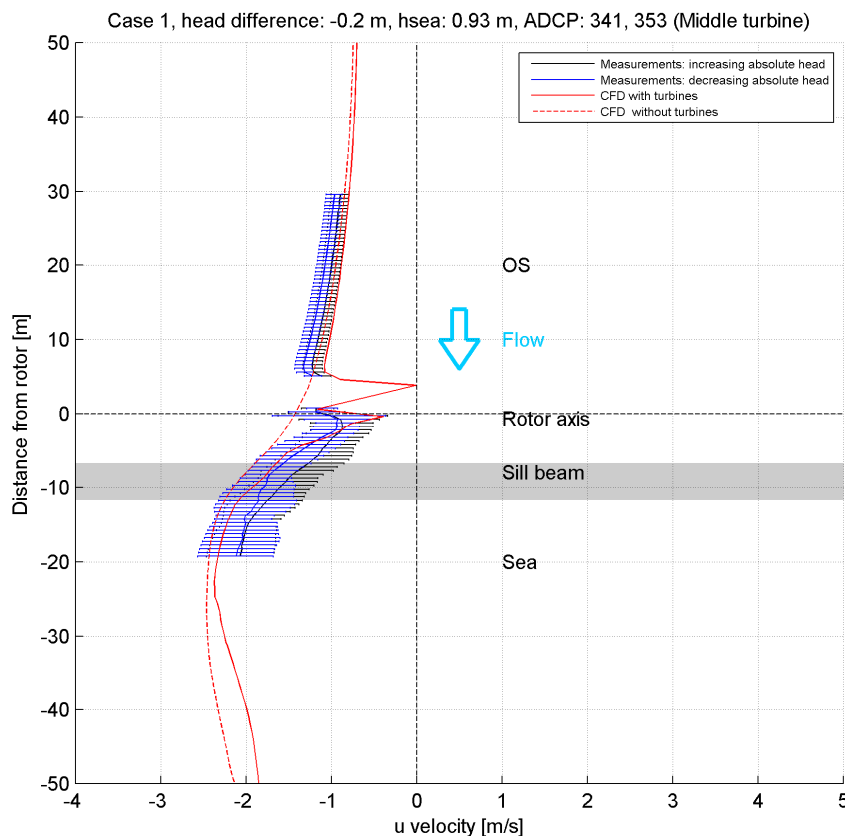


Figure 3.15 Longitudinal ADCP profile from the measurements with turbines – comparison between CFD and measurements – Ebb Case WT. 1. For illustrative purposes, the profile along the same line is also plotted for the corresponding simulation without turbines NT. 1

For the flood case (Figure 3.16) the inflow profile is at the bottom of the graph showing the flow acceleration towards the barrier. In the flood case the velocity magnitude is lower compared to the measurements and the difference is greater than in the ebb case. The difference with the simulation without turbines is less in this case but is still consistent with extra resistance from the turbines. However, even the CFD simulation without turbines shows lower inflow velocities than the measurements of velocity with turbines for the same case. This is inconsistent and given that the velocities without turbines have been well validated against the 2011 measurements less throws some doubt on the absolute values of the 2016

measurements. In the analysis of the measurements (ref [31]), it was observed that the flow velocity during flood is about 5-10% larger for the situation with turbines than for the situation without turbines.

In the wake region the recovery of the velocity is faster in the CFD model than in the measurements. For the flood case the wake region is much larger than in the ebb case because the flow is not subsequently squeezed through the barrier. The recovery is not complete after 50 m (note that the CFD domain extends 200 m downstream of the barrier).

The agreement of the CFD with the measurements is acceptable. Some of the details of the flow patterns are not predicted correctly, such as the distance of the wake recovery and from the comparison of the velocity profiles it can be concluded that the CFD slightly underestimates the discharge. This could be attributed to the lack of sufficient mesh resolution in the wake region in order to model the turbulence in this region. An analysis of the turbulent scales which have been resolved by the simulations has been made in [33].

The velocity profiles for the remaining cases (NT.2 and NT.3) are presented in Appendix C.

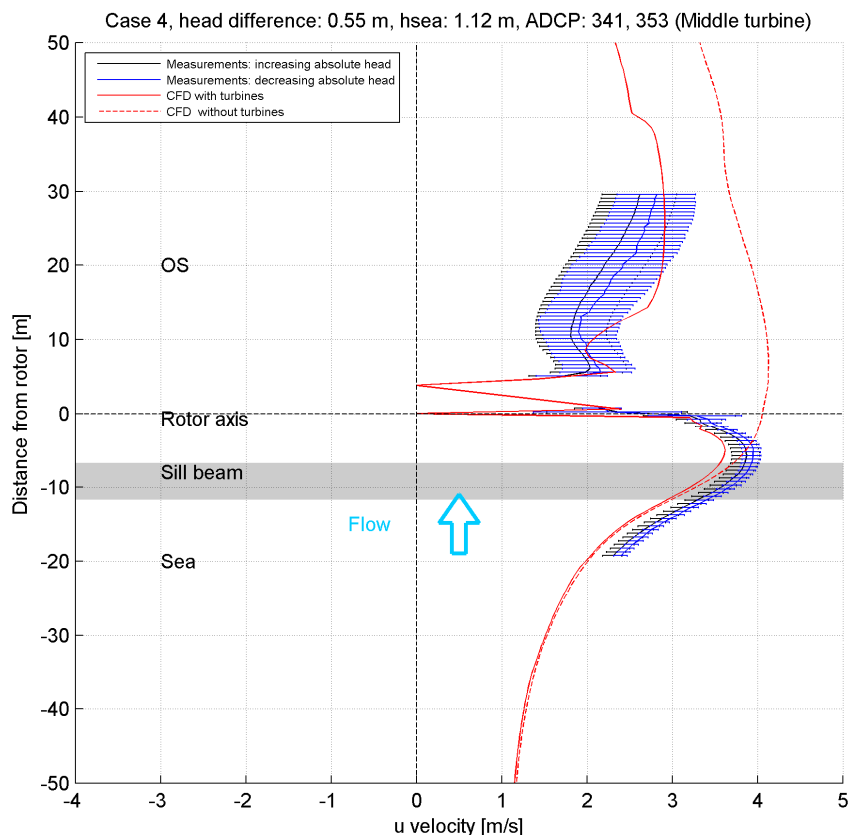


Figure 3.16 Longitudinal ADCP profile from the measurements with turbines – comparison between CFD and measurements – Flood Case WT.4. For illustrative purposes, the profile along the same line is also plotted for the corresponding simulation without turbines NT.4

3.2.3 Discharge coefficients

The discharge coefficients from the simulations, as defined in Section 0, were calculated for each CFD case. A distinction is made for a coefficient over the whole domain and between each port of the barrier. For the simulations with turbines these will differ owing to the

resistance that the turbines have on the flow. The discharges for the whole domain are calculated at the boundary. The Star-CCM+ monitors give a constant discharge at the inlet boundary, owing to the specification of the inlet profile there. The discharge at the outlet boundary varies during the simulation owing to the unsteadiness of the flow. The value reported in Table 3.2 is based on the value at the inlet. The discharges for the flow through the port and sides are based on an average in time of the flow through a cross-section at the barrier.

Table 3.2 Summary of the results for the discharge coefficients for the simulations with turbines

	Case	Water Level [m NAP]		Head [m]	Discharge			μ		
		North Sea	Eastern Scheldt		Domain	Port	Side	Domain	Port	Side
				[m ³ /s]	[m ³ /s]	[m ³ /s]	[-]	[-]	[-]	
Ebb	WT.1	0.93	1.12	-0.19	1489	730	766	0.94	0.93	0.97
	WT.2	0.68	1.00	-0.32	1894	925	980	0.94	0.92	0.98
Flood	WT.3	-0.57	-0.78	0.21	1174	588	587	0.85	0.85	0.85
	WT.4	1.11	0.57	0.54	2278	1140	1140	0.88	0.88	0.88

By comparing the discharge coefficients from the situation with turbines (Table 3.3) with the situation without turbines, it is seen that the discharge coefficient for ebb reduces more than that for flood. The percentage difference for an ebb case is approximately 5% and for flood the difference is negligible.

Table 3.3 Comparison of the results for the discharge coefficients of the ports with and without turbines

	Case	Head [m]	μ without turbines	μ with turbines	Δ %
			Side	Port	
			[-]	[-]	
Ebb	1	-0.19	0.97	0.93	5%
	2	-0.32	0.98	0.92	6%
Flood	3	0.21	0.85	0.85	0%
	4	0.54	0.88	0.88	0%

3.2.4 Turbine power

Tocado controls the operation of the turbines in the Eastern Scheldt Storm Surge Barrier based on the rotational speed of the turbine. The rotational speed of the turbine will be tuned in such a way that the maximum amount of energy can be subtracted from the turbine. This maximum efficiency point of the turbine appears at a tip speed ratio of 4.3. This means that the ADCPs are not used to control the turbine operation.

In the CFD model, the rotational speed of the turbines is used as an input parameter. Together with the torque of the turbine, the power is calculated via the formula: $P = \tau\omega$, in which τ is the torque (Nm) and ω is the angular velocity [rad/s]. The generated power is compared with the measured power from Tocardo. The measured power is the power that has been delivered to the grid. Tocardo provided a conversion relation between the grid power and the power on the rotor. This relation is presented in Figure 3.17. Due to energy losses, the power on the rotor is approximately 10% higher.

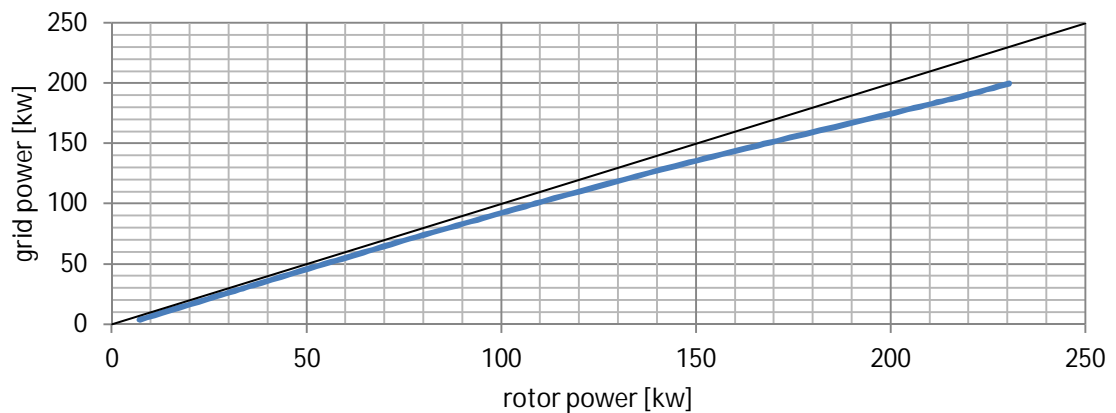


Figure 3.17 Relation (blue) between the power on the rotor and the power that has been delivered to the grid. (black line represents no losses 1:1 relation)

In Table 3.4, the obtained power by the CFD model is presented in combination with the difference with the modelled power. The deviation on the mean velocity for the higher power output cases is below 10%. It has to be noted that the standard deviation for the modelling results is in the order of 5-10% of the mean power. For the measurements, the standard deviation of the power is in the order of 10-20%, with lower standard deviations for the cases with the larger head difference. Based on this analysis, it is concluded that the CFD model represents the measured power well.

Table 3.4 Summary of the CFD results for the power from the turbines

	Case number	modelled power					Difference between modelled & measured power				
		T12-1 [kW]	T14-2 [kW]	T11-3 [kW]	T15-4 [kW]	T09-5 [kW]	T12-1 [kW]	T14-2 [kW]	T11-3 [kW]	T15-4 [kW]	T09-5 [kW]
Ebb	WT.1	9.1	9.8	10.6	10.7	12.0	-4.7	-2.9	-0.7	-1.6	2.1
	WT.2	19.8	20.8	22.2	22.5	24.8	-12.7	-10.3	-7.6	-8.5	-4.6
Flood	WT.3	49.0	48.4	48.6	48.4	48.5	2.8	1.6	4.7	2.5	1.7
	WT.4	218.2	201.5	197.9	199.4	208.8	27.2	7.6	11.9	10.6	16.1

3.2.5 Thrust

The thrust, which is obtained from the CFD model is presented in Table 3.5. The differences with the measured values is approximately 10kN. For the case with higher forcing on the turbines WT.4, the relative difference is maximum 5% of the measured thrust. Similar to the power, the standard deviation of the modelling results is 5%, while the standard deviation of the measurements is in the order of 10-30%. Where the cases with the lower head difference show the larger standard deviations. From this analysis, it is concluded that the CFD model represents the measured thrust sufficiently accurate.

Table 3.5 Summary of the CFD results for the thrust on the turbines

	Case number	modelled thrust					Difference between modelled & measured thrust				
		T12-1 [kN]	T14-2 [kN]	T11-3 [kN]	T15-4 [kN]	T09-5 [kN]	T12-1 [kN]	T14-2 [kN]	T11-3 [kN]	T15-4 [kN]	T09-5 [kN]
Ebb	WT.1	-12.2	-12.8	-13.4	-13.5	-14.4			6.6		11.0
	WT.2	-23.1	-23.9	-24.8	-25.1	-26.5			9.1		13.6
Flood	WT.3	38.5	38.6	38.5	38.6	38.5			-4.7		-6.9
	WT.4	114.6	111.4	110.6	110.9	113.5			5.6		-4.2

4 Discussion

4.1 Validation of the model

The CFD model has been validated against field measurements taken from ADCPs mounted at the barrier during operation. The agreement in velocity at the ADCP profile locations is good for the cases and head differences studied. The agreement is better for the ADCP measurements taken in the situation without turbines. For the situation with turbines the inflow velocities are slightly underpredicted. This could indicate that the discharges are also slightly underpredicted in the case with turbines. However, it has to be noted that the field measurements of the situation with turbines showed about 5-10% higher velocities than for the situation without turbines (ref [31]). Similarly the details of some of the profiles, the size of the recirculation zone and the size of the wake recovery zone, show some discrepancies but for the bulk parameter of a discharge coefficient this is of less importance. Also in general the good agreement between the measurements and the CFD give confidence that the quality of the predicted flow field is high.

The predictions of the power and thrust from the turbines are validated as well. For both parameters, the standard deviation of the measurements is significant (between 10% and 30%). The agreement with the measurements at the high flow rate (WT.4) is quite good (<10%). This may mean the model performs well for the prediction of the optimal location of the turbines in the flow field for power generation.

4.2 Inclusion of rotating zones around the turbines

The largest uncertainty in the results of the CFD simulations is created by the rotating zones around the turbines. The earlier validation [3] of the CFD model with turbines was performed with a larger rotating zone around the turbines than was possible to apply in these simulations. A larger zone is generally preferable because it allows the interpolation between rotating and stationary zones to be made at a location where the gradients are small and the numerical errors will similarly be smaller. For the simulations of 5 turbines in a row in the opening of the barrier it is not possible to create a larger zone. Similarly for the flood case, the location of the rotating zone in a region of very high gradients downstream of the flow separation at the sill, makes the numerical errors of interpolation greater. The expected effect of this is to increase so called numerical diffusion which is a form of extra resistance in simulations which are not fully resolved.

The inclusion of the rotating turbines in the simulations is state-of-the-art (see discussion of literature in Section 1.1). The validation performed here with the turbines shows that this model is possible of generating validated mean profiles whilst still resolving a large proportion of the unsteady turbulence generated by the turbines and thereby giving insights into the true effect of the turbines on the downstream flow.

4.3 Biofouling of the Eastern Scheldt Barrier

During installation of the horizontal and vertical ADCP's in 2011 by Partrac, biofouling was observed on the sill. A layer of approximately 10cm of shells had to be removed from the sill before installation of the ADCP equipment. This layer of biofouling has not been included in the CFD simulations, while it has an effect on the flow through the barrier.

Some simulations with different roughness were made during the validation process of the model but adding a roughness as much as 10 cm is not possible in the current setup because

in the model currently used the roughness is limited to the size of the first cell near the wall. An investigation of other methods to include roughness in the model was not carried out.

4.4 Inertia effects in the Eastern Scheldt

From the measurements (ref [31]) it became clear that due to inertia, the velocities are much higher at the end of the tidal phase than at the beginning of the tidal phase. This effect is not included in the CFD model because the water levels were imposed as constant boundary conditions. The CFD simulations also do not include the oblique approach flow which is present at the start of the tidal phase for the ebb cases (see Figure 2.11). This oblique flow is a result of inertial effects in the Eastern Scheldt owing to the tidal variations. This oblique approach flow angle could have an effect on the validation of the power measurements.

4.5 Possible discrepancy in velocity measurements

In the report of the field measurements (ref [31]) an analysis has been made of the agreement between the measurements made in 2011 and 2016. The conclusion was made that the measurements seemed consistent near the barrier although in the flood case the velocities in the measurements with turbines were approximately 5% higher than without turbines. The comparison was difficult to make because there was no common measurement point in the two campaigns and this analysis was made at only one location for each dataset.

The CFD model provides data over the entire domain. Comparisons with the CFD shown in the previous sections show that the agreement with the measurements in 2011 is good and that the comparison of the CFD with and without turbines shows a logical consistency. The velocities and discharges with turbines are always less than without turbines, owing to the resistance of the turbines.

However, there does appear an inconsistency with the measurements of 2016 for the inflow velocities. In for instance Figure 3.16 the inflow velocities of the two CFD cases show lower values than the measurements. This would suggest that the discharges in the simulations are lower: even in the simulation without turbines. However this simulation shows good agreement with the velocity measurements from 2011 (and therefore the calculated discharge).

It is unclear how the measurements with turbines in 2016 could give a higher measured inflow velocity and therefore discharge than the validated CFD model without turbines for the same case. Owing to the agreement and consistency of CFD and results from 2011 it seems that the accuracy of the inflow velocities from 2016 far from the ADCP is questionable.

5 Conclusions

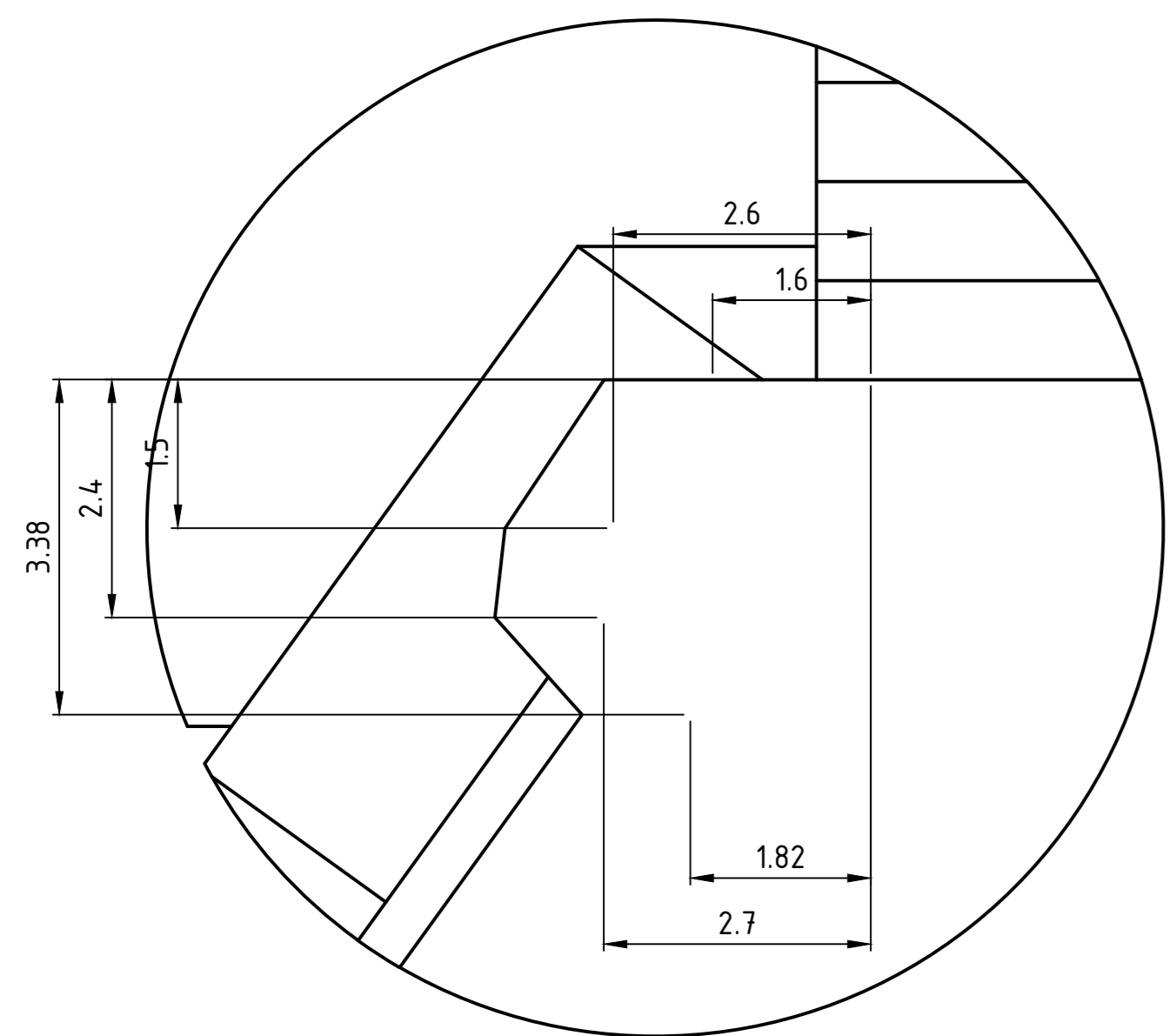
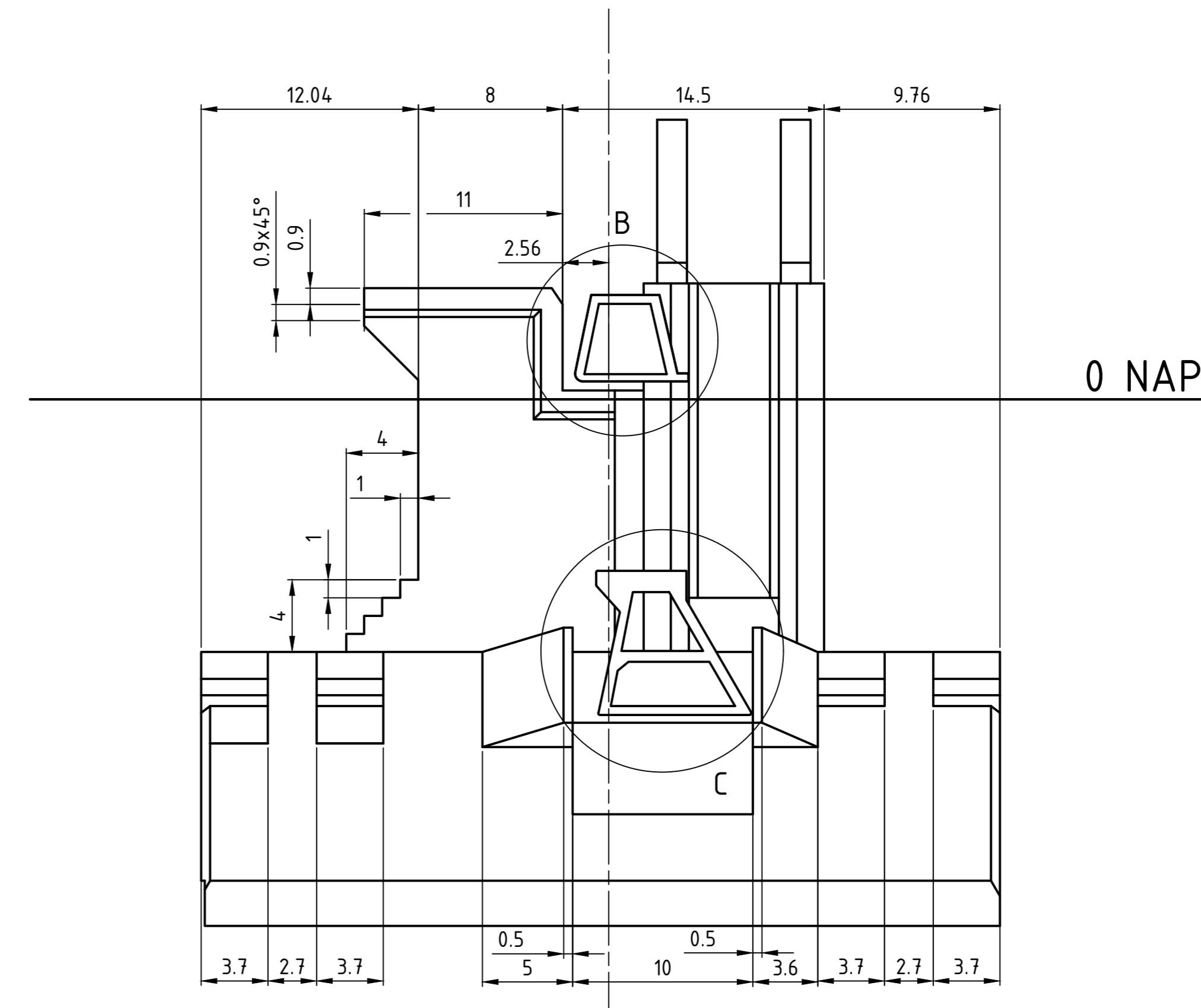
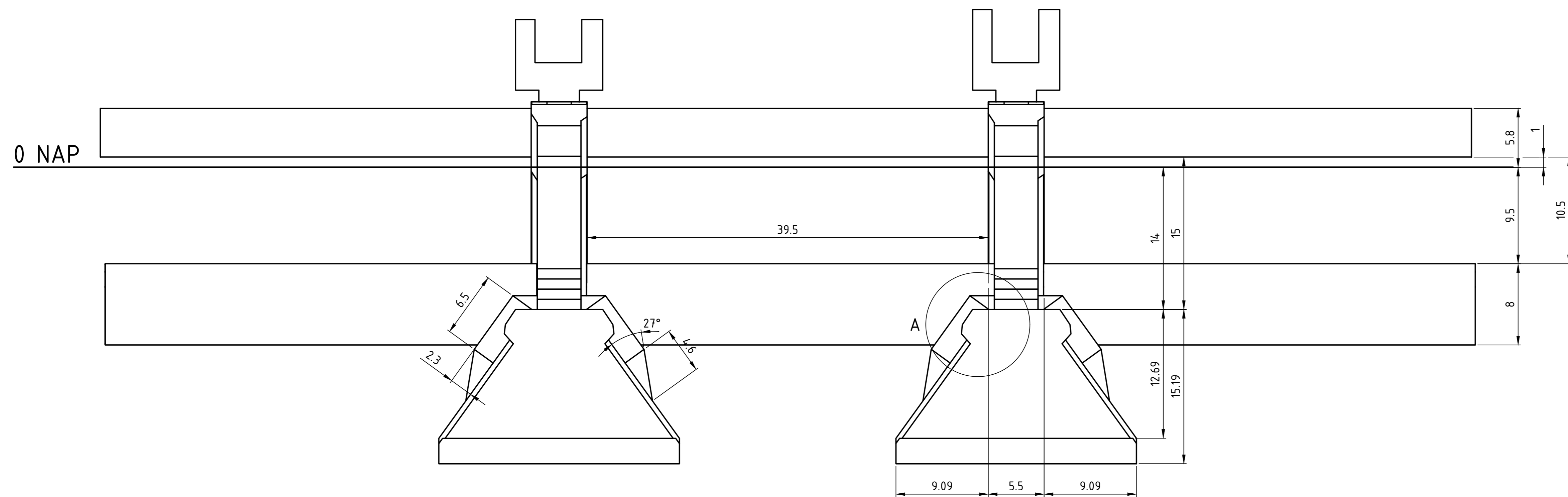
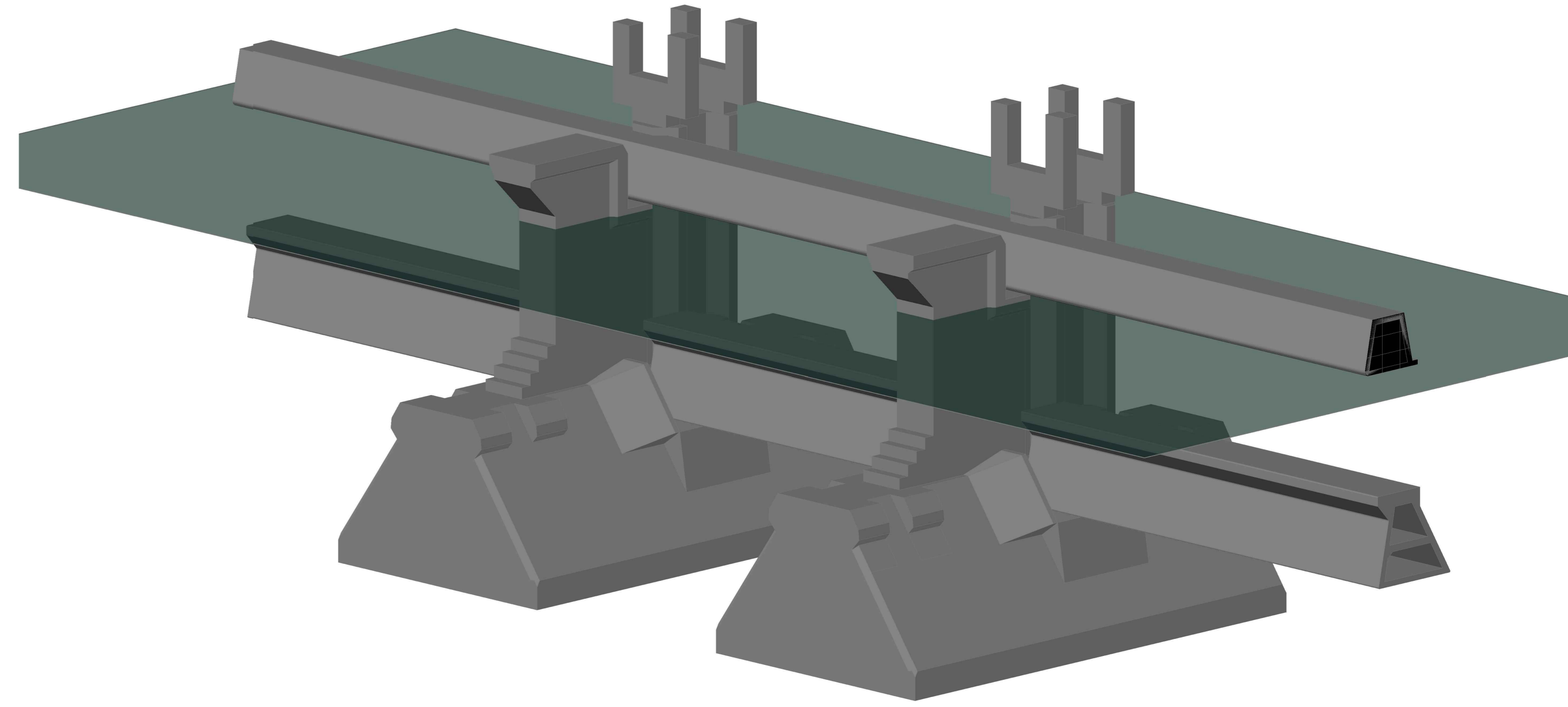
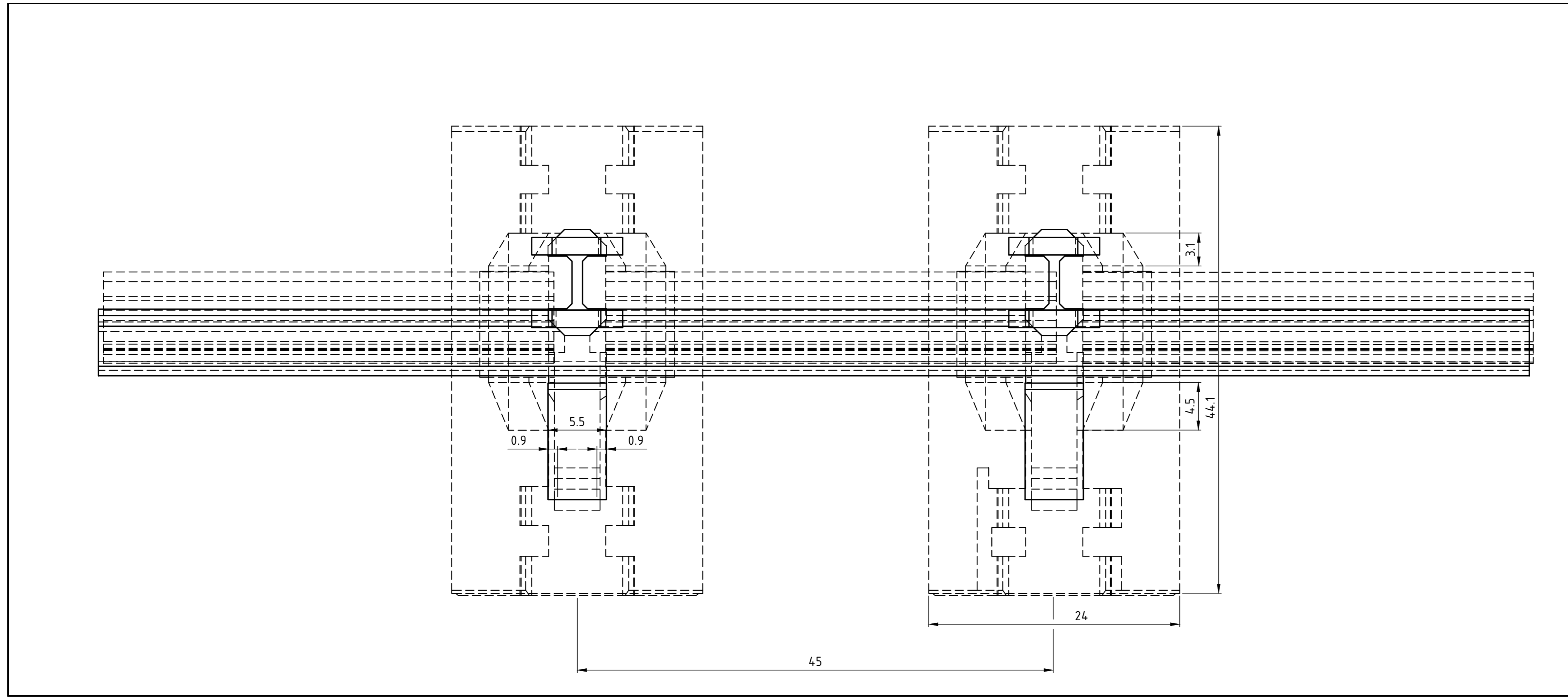
The CFD simulations performed of the Eastern Scheldt Barrier were conducted for the purpose of the prediction of discharge capacity and flow patterns downstream of the barrier (see Objective in 1.2). With this objective in mind the following conclusions can be drawn:

- 1) Effect of turbines on discharge coefficient: the turbines have only a small effect on the discharge coefficients. For the ebb case the reduction in discharge coefficient between simulations without and with turbines is approximately 5%. For the flood cases the reduction was negligible in both cases but this is likely within the range of accuracy of the simulations. The small effect on the discharge coefficient for flood is attributed to the fact that the turbines are placed sufficiently far from the sill. During ebb, the turbines are upstream of the barrier, which causes a reduced discharge coefficient.
- 2) Model is validated for discharge coefficients: the agreement between the CFD and ADCP field measurements of velocity profiles is good. The small discrepancy in a number of details is not sufficient to result in significant differences in the total flow through the barrier. The agreement in the profiles is also not sensitive to the exact location in the domain at which the profile is drawn. This gives confidence that the comparison made is valid for a large part of the flow field. For the cases with turbines it appears that the inflow velocities (and consequently discharges) are slightly underpredicted. However, it is unclear if this is caused by the numerical model or by the flow measurements (ref [31]), which have shown that the upstream flow velocities are higher for the situation with turbines than without turbines. It is concluded that the developed model is suitable for an assessment of the effect of the turbines on the discharge coefficient.
- 3) Model validation for power and thrust still is carried out as well: the discrepancy between the CFD calculated turbine power and the measured turbine is small for high discharges and within the ranges of uncertainty. For simulations where the agreement in inflow velocity profiles is better the agreement with the measured power is also improved. This may mean the model performs well for the prediction of the optimal location of the turbines in the flow field for power generation.

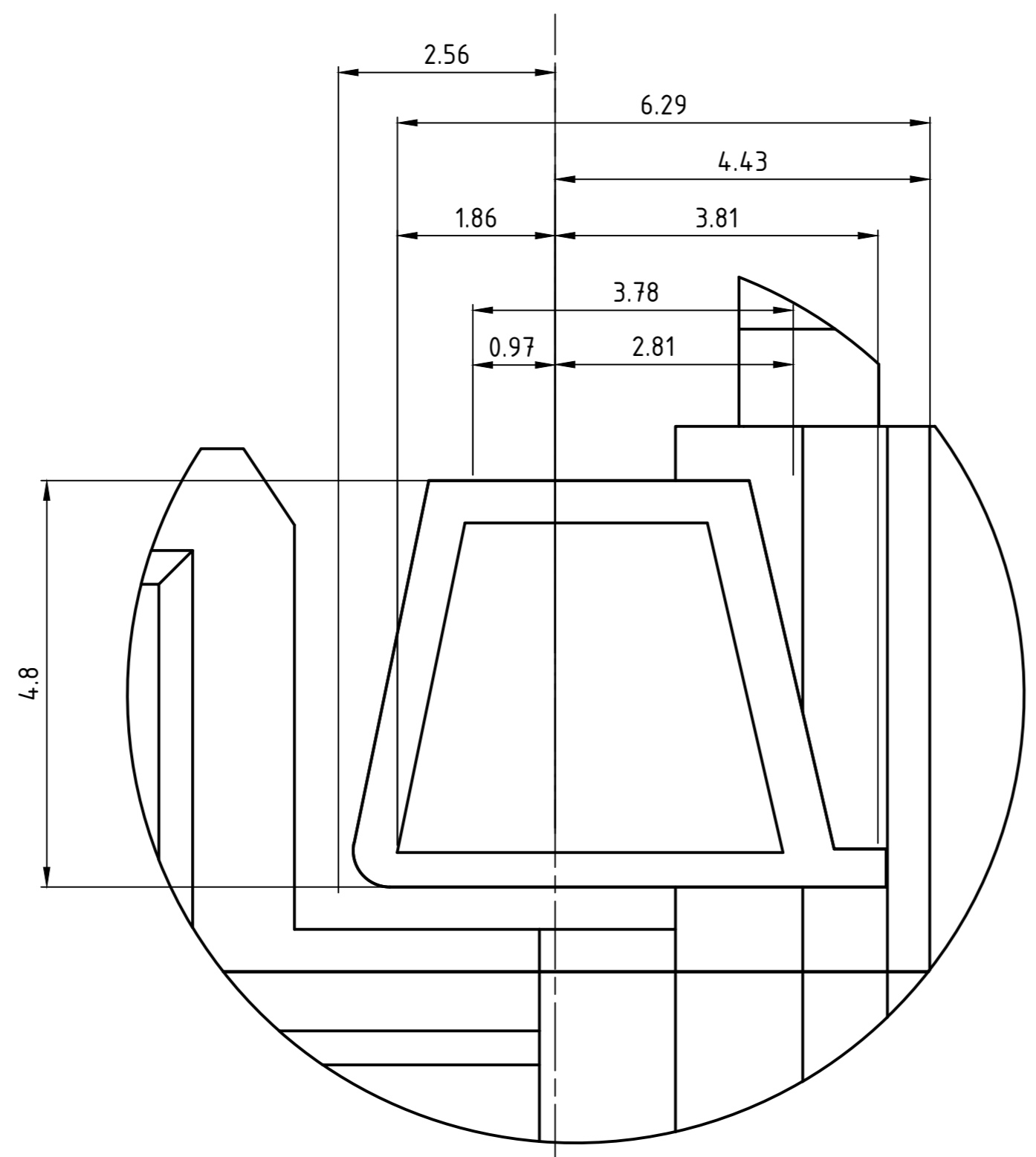
6 References

1. Fockert, A.d., *Environmental impact of tidal energy plant in Eastern Scheldt Storm Surge Barrier*. 2018, Deltares.
2. Rijkswaterstaat, *Design Plan Oosterschelde Storm Surge Barrier: Overall design and design philosophy*. 1994, Rijkswaterstaat: Rotterdam, The Netherlands.
3. Tralli, A., et al., *CFD Study on Free-Surface Influence on Tidal Turbines in Hydraulic Structures*. Proc. of the ASME 34th International Conference on Ocean, Offshore and Arctic Engineering, 2015(OMAE2015-41187).
4. Bijlsma, A., et al., *Detailed dynamics of the Eastern Scheldt storm surge barrier: validation of a CFD approach*. Proc. of the 4th International Symposium of Shallow Flows, 2017.
5. Batten, W.M.J., et al., *The prediction of the hydrodynamics performance of marine current turbines*. Renewable Energy, 2008. **33**: p. 1085-1096.
6. Turnock, S.R., et al., *Modelling tidal current turbine wakes using a coupled RANS-BEMT approach as a tool for analysing power capture of arrays of turbines*. Ocean Engineering, 2011. **38**: p. 1300-1307.
7. Jo, C.H., et al., *Performance of horizontal axis tidal current turbine by blade configuration*. Renewable Energy, 2012. **42**: p. 195-206.
8. Gant, S. and T. Stallard, *Modelling a tidal turbine in unsteady flow*. Proc. 18th Int. Offshore and Polar Engineering Conference, 2008: p. 473-480.
9. Batten, W.M.J., M.E. Harrison, and A.S. Bahaj, *Accuracy of the actuator disc-RANS approach for predicting the performance and wake of tidal turbines*. Phil Trans R Soc A, 2013. **371**(20120293).
10. Myers, L. and A.S. Bahaj, *Power output performance characteristics of a horizontal axis marine current turbine*. Renewable Energy, 2005. **31**: p. 197-208.
11. Myers, L. and A.S. Bahaj, *Wake studies of a 1/30th scale horizontal axis marine current turbine*. Ocean Engineering, 2007. **34**: p. 758-762.
12. Sun, X., J.P. Chick, and I.G. Bryden, *Laboratory-scale simulation of energy extraction from tidal currents*. Renewable Energy, 2008. **33**: p. 1267-1274.
13. Myers, L. and A.S. Bahaj, *Experimental analysis of the flow field around horizontal axis tidal turbines by use of scale mesh disk rotor simulators*. Ocean Engineering, 2010. **37**(218-227).
14. Harrison, M.E., et al., *A comparison between CFD simulations and experiments for predicting the far wake of horizontal axis tidal turbines*. Proc. 8th European Wave and Tidal Energy Conference (EWTEC), 2010.
15. Lawson, M.J., Y. Li, and D. Sale, *Development and Verification of a Computational Fluid Dynamics Model of a Horizontal Axis Tidal Current Turbine*. Proc. 30th ASME Int. Conf. on Ocean, Offshore and Arctic Engineering, 2011(OMAE2011-49863).
16. Otto, W., D. Rijpkema, and G. Vaz, *Viscous Flow Calculations on an Axial Marine Current Turbine*. Proc. 31th ASME Int. Conf. on Ocean, Offshore and Arctic Engineering, 2012(OMAE2012-83452).
17. Mason-Jones, A., et al., *Non-dimensional scaling of tidal stream turbines*. Energy, 2012: p. 820-829.
18. Frost, C., et al., *The effect of tidal flow directionality on tidal turbine performance*. Renewable Energy, 2015. **78**: p. 609-620.
19. Bahaj, A.S., W.M.J. Batten, and G. McCann, *Experimental verification of numerical predictions for the hydrodynamic performance of horizontal axis marine current turbines*. Renewable Energy, 2007. **32**: p. 2479-2490.
20. Bahaj, A.S., et al., *Power and Thrust measurements of marine current turbines under various hydrodynamic flow conditions in a cavitation tunnel and towing tank*. Renewable Energy, 2007. **32**(3): p. 407-426.
21. Whelan, J., J.M.R. Graham, and J. Peiro, *A free-surface and blockage correction for tidal turbines*. Journal of Fluid Mechanics, 2009. **624**: p. 281-291.
22. Consul, C.A., R.H.J. Willden, and S.C. McIntosh, *Blockage effects on the hydrodynamic performance of a marine cross-flow turbine*. Phil Trans R Soc A, 2013. **371**(20120299).
23. Blackmore, T., W.M.J. Batten, and A.S. Bahaj, *Influence of turbulence on the wake of a marine current turbine simulator*. Phil Trans R Soc A, 2014. **470**(20140331).
24. Blackmore, T., L. Myers, and A.S. Bahaj, *Effects of turbulence on tidal turbines: Implications to performance, blade loads and condition monitoring*. International Journal of Marine Energy, 2016. **14**: p. 1-26.
25. Churchfield, M.J., Y. Li, and P.J. Moriarty, *A large-eddy simulation study of wake propagation and power production in an array*. Phil Trans R Soc A, 2013. **371**(20120421).
26. Daly, T., L. Myers, and A.S. Bahaj, *Modelling of the flow field surrounding tidal turbine arrays for varying positions in a channel*. Phil Trans R Soc A, 2013. **371**(20120246).
27. Stallard, T., et al., *Interactions between tidal turbine wakes: experimental study of a group of three-bladed rotors*. Phil Trans R Soc A, 2013. **371**(20120159).
28. Olczak, A., et al., *Comparison of a RANS blade element model for tidal turbine arrays with laboratory scale measurements of wake velocity and rotor thrust*. Journal of Fluids and Structures, 2016. **64**: p. 87-106.
29. O'Doherty, T., et al., *Considerations of a horizontal axis tidal turbine*. Proc. Inst of Civil Engineers. Energy, 2010. **163**(EN3): p. 119-130.
30. Ahmed, U., et al., *CFD simulations of a full-scale tidal turbine: comparison of LES and RANS with field data*. Proc. 11th European Wave and Tidal Energy Conference (EWTEC), 2015.
31. Verbruggen, W., *Analysis ADCP data Eastern Scheldt Barrier with and without turbine deployment*. 2018, Deltares.
32. Guijt, K., *Impact of Tidal Energy Extraction in the Eastern Scheldt Surge Barrier on Basin Hydrodynamics and Morphology*, in *Hydraulic Engineering*. 2018, TU Delft.
33. Stevens, T., *The prediction of stone stability by a three-dimensional eddy resolving simulation technique*, in *Hydraulic Engineering*. 2018, TU Delft.

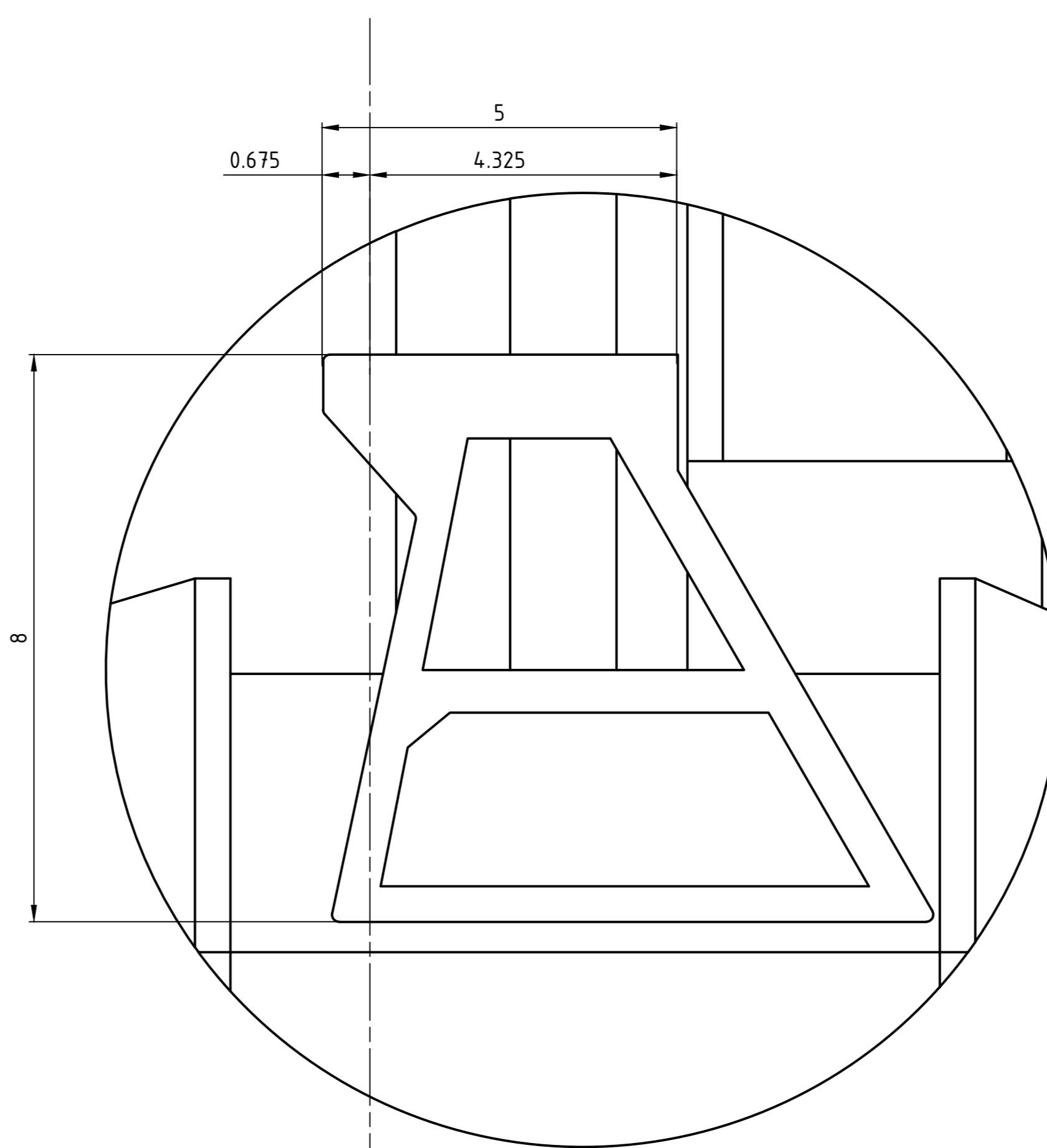
A Detailed drawings of the geometry and turbines as present in the CFD model



Detail A

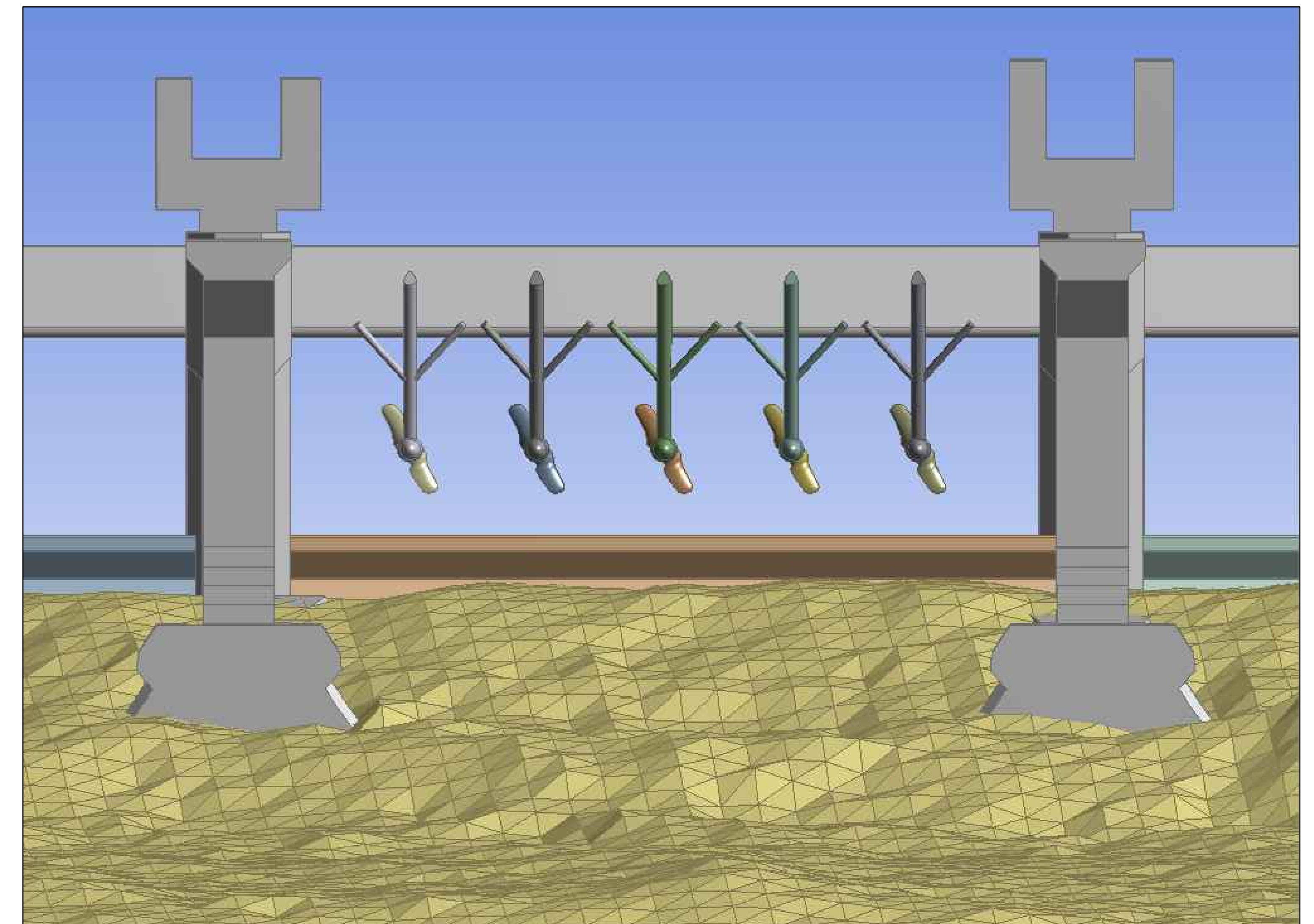
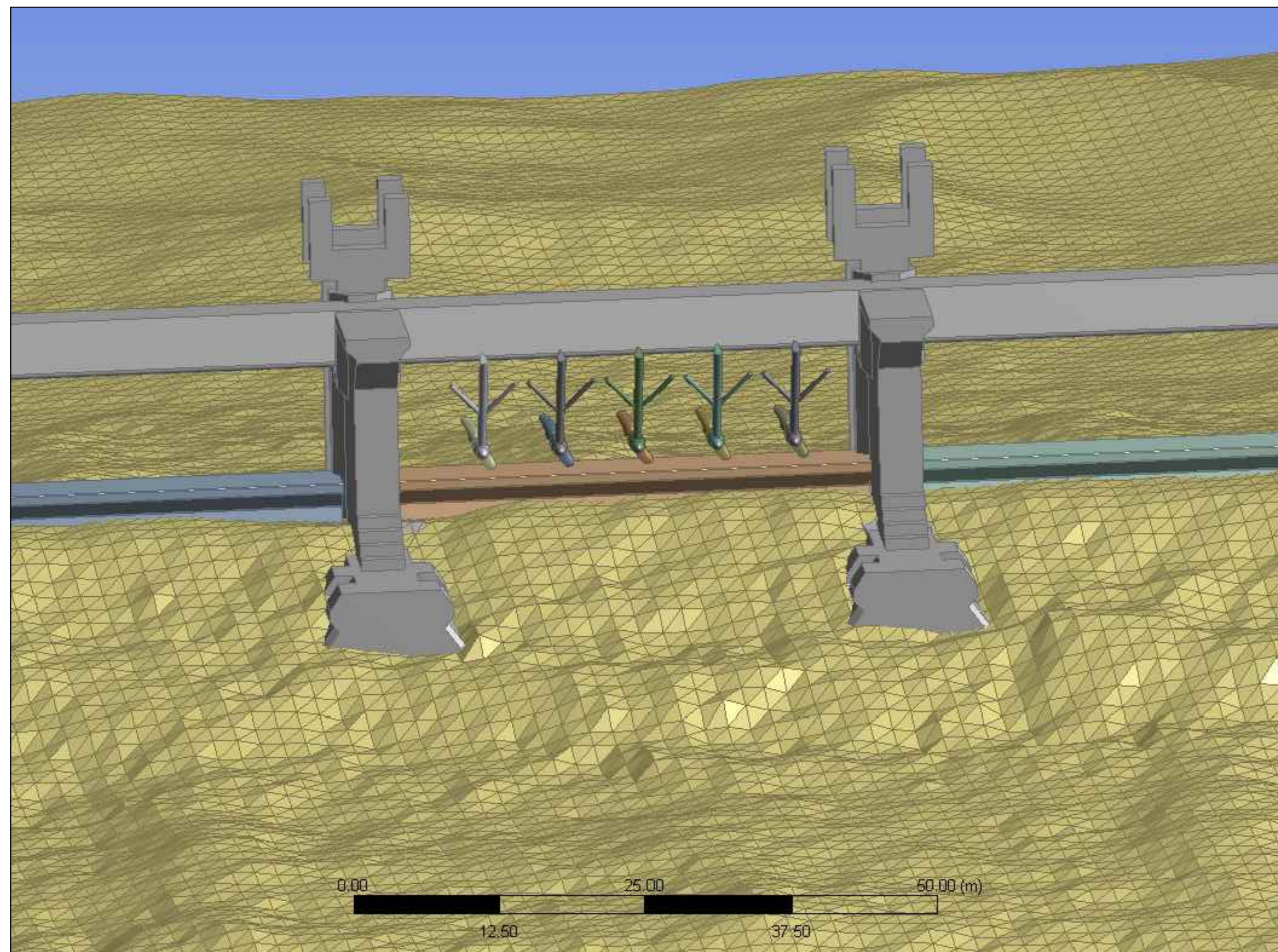
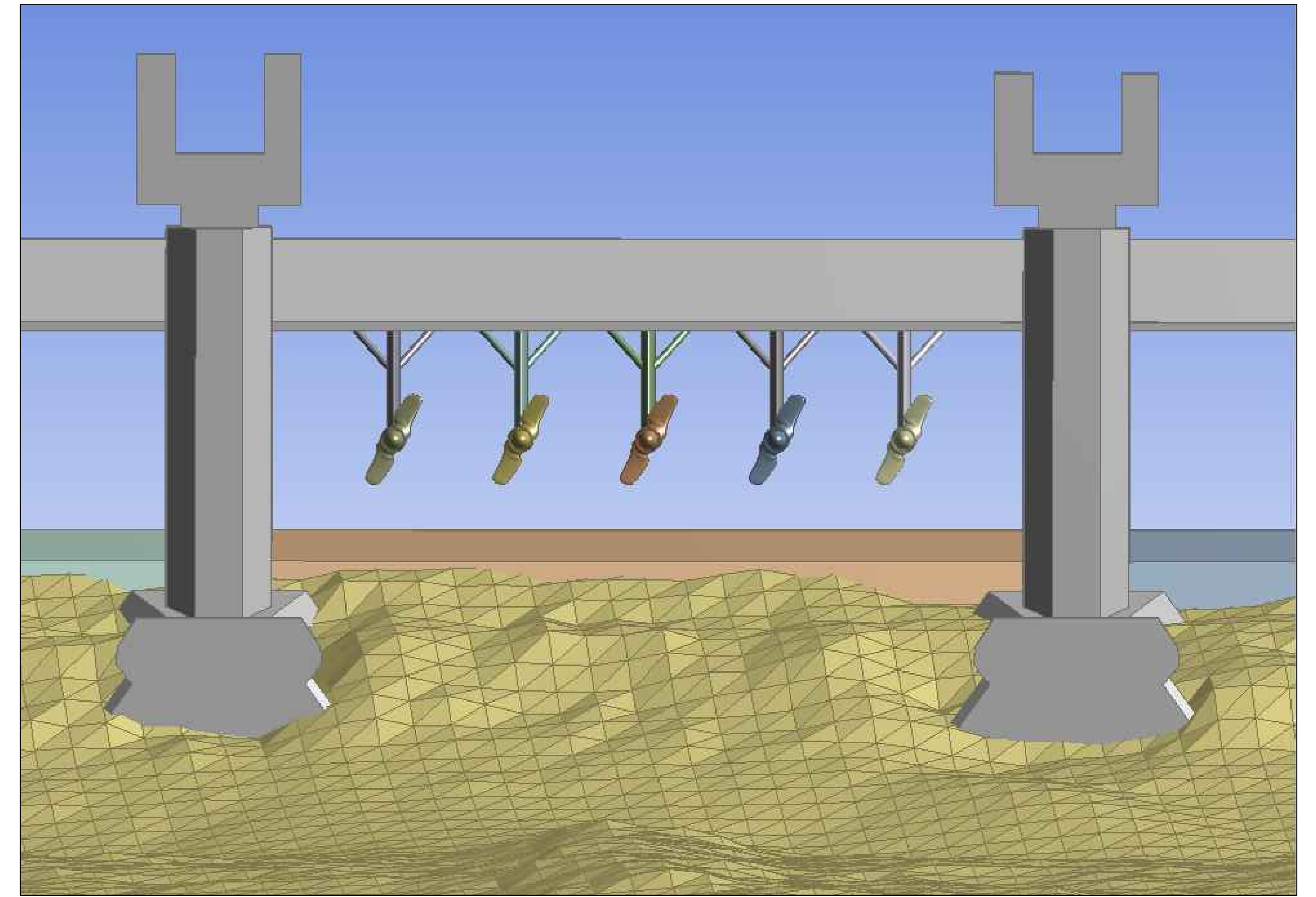
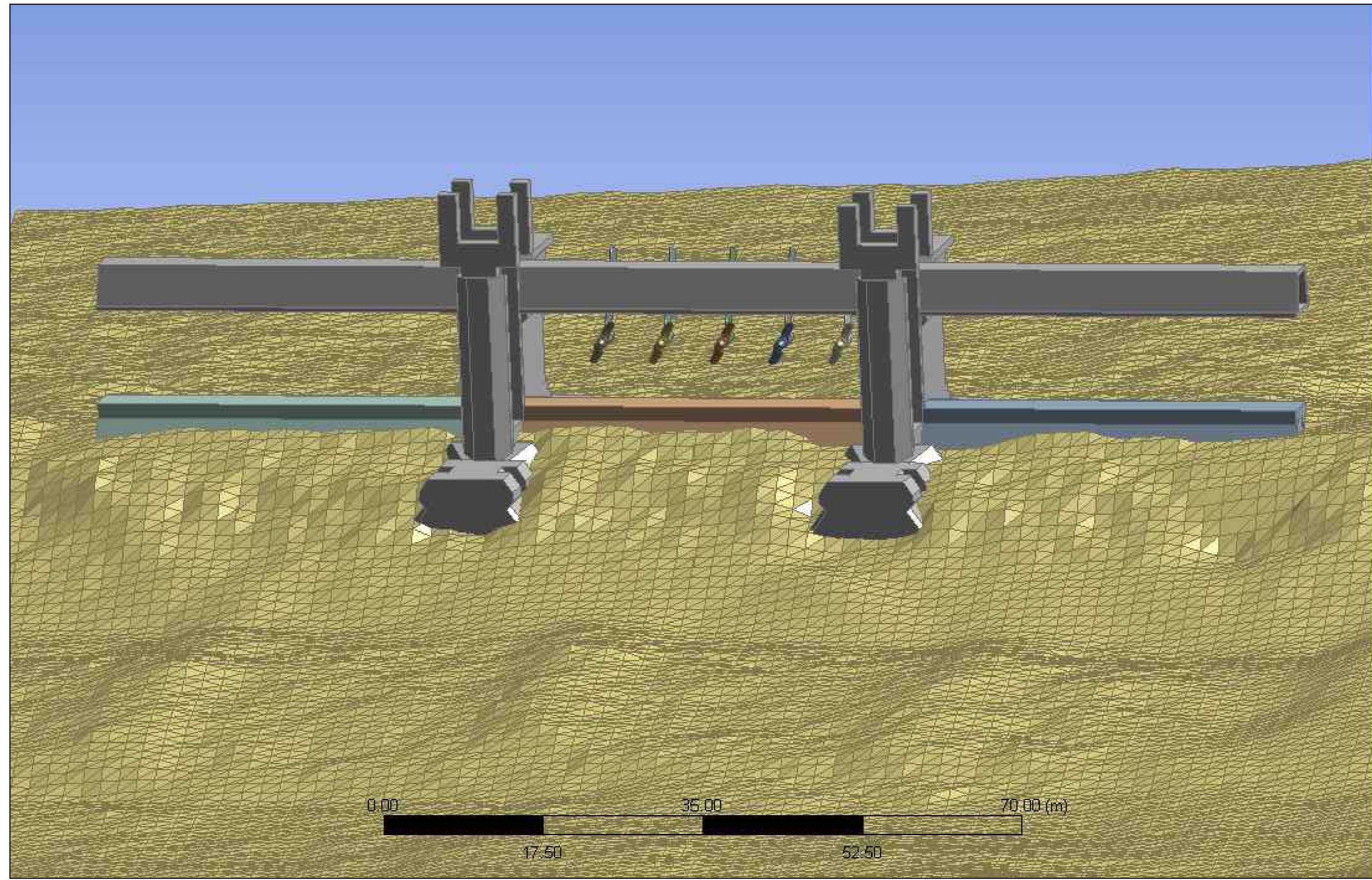


Detail B



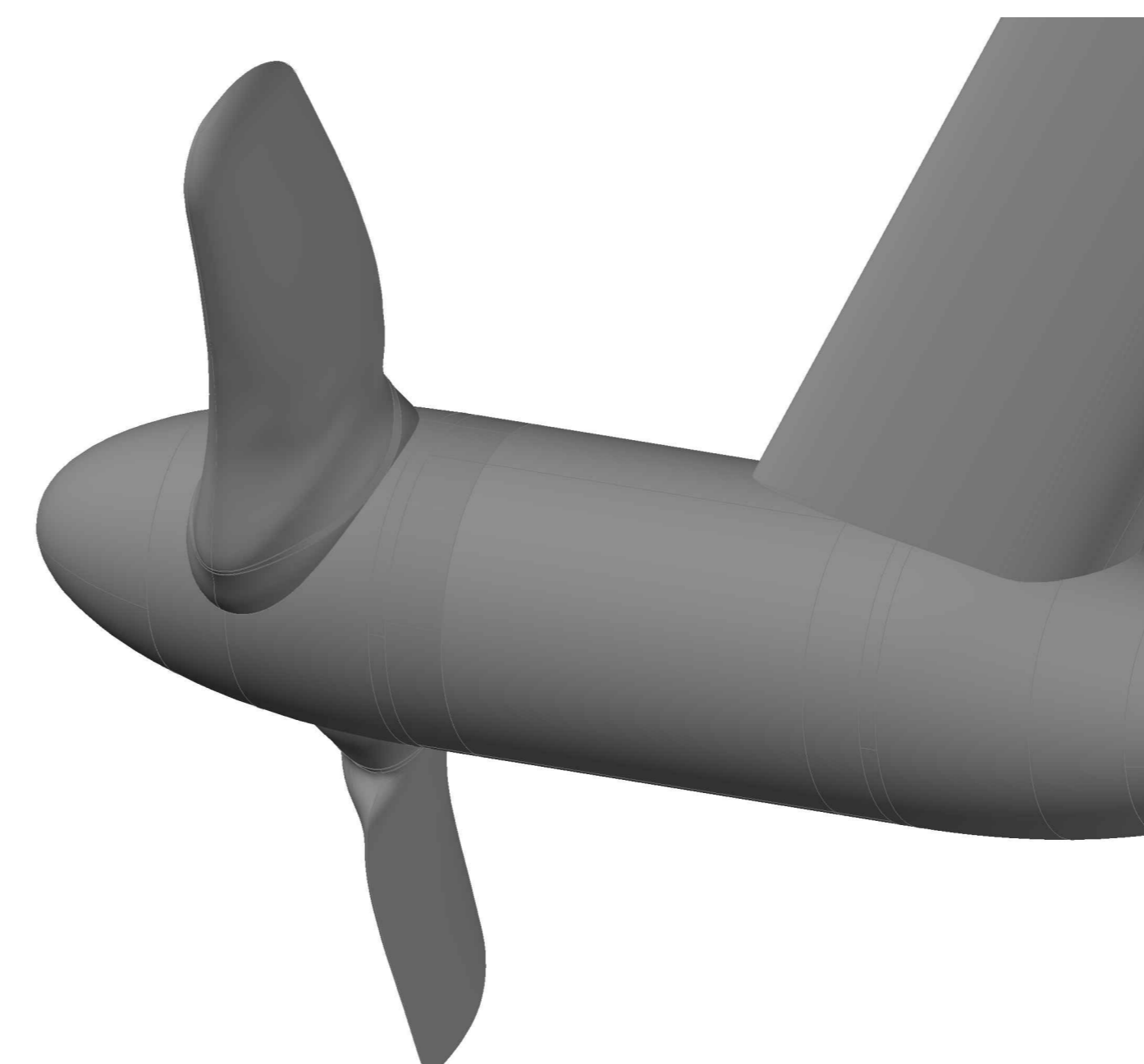
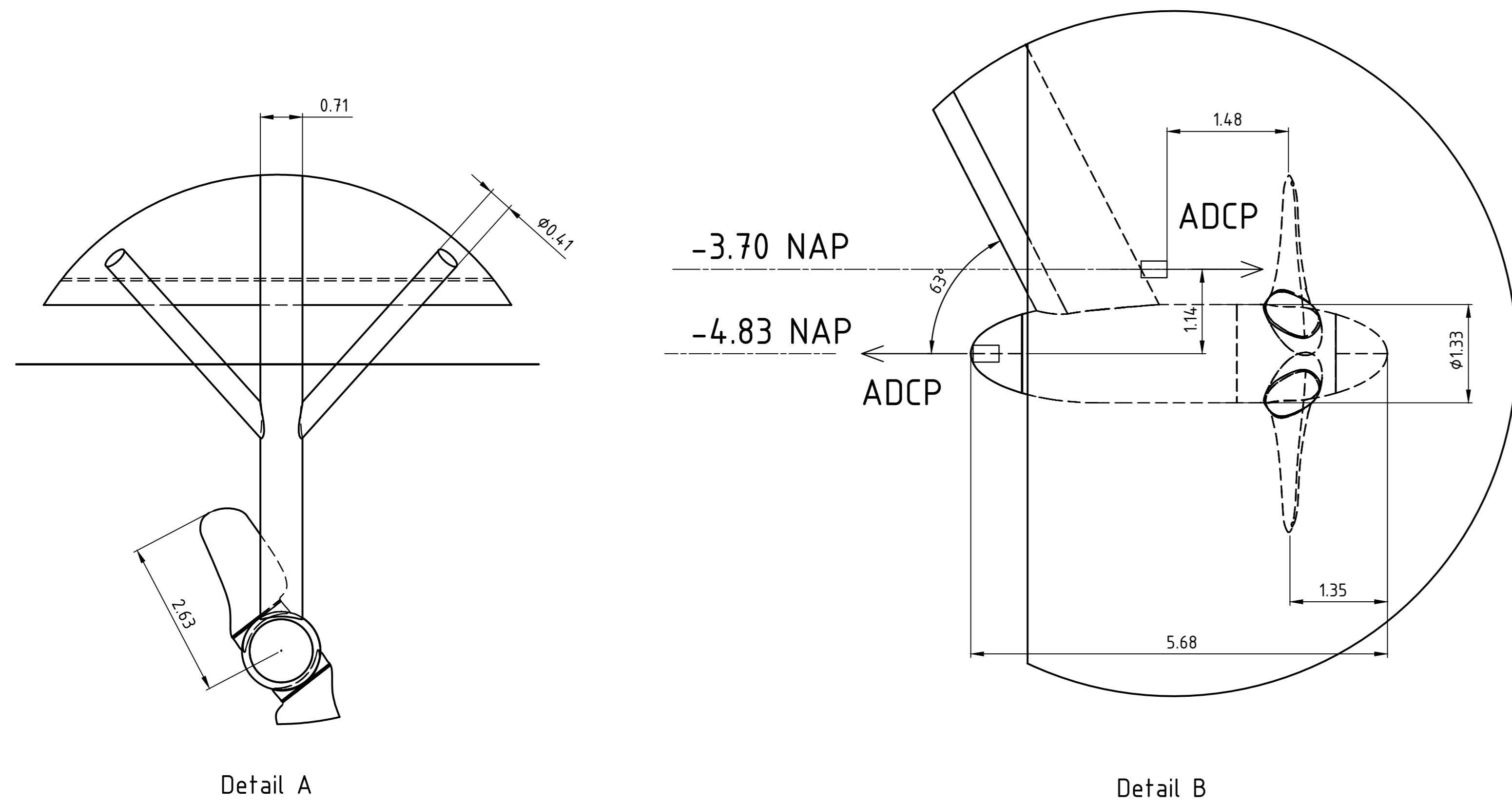
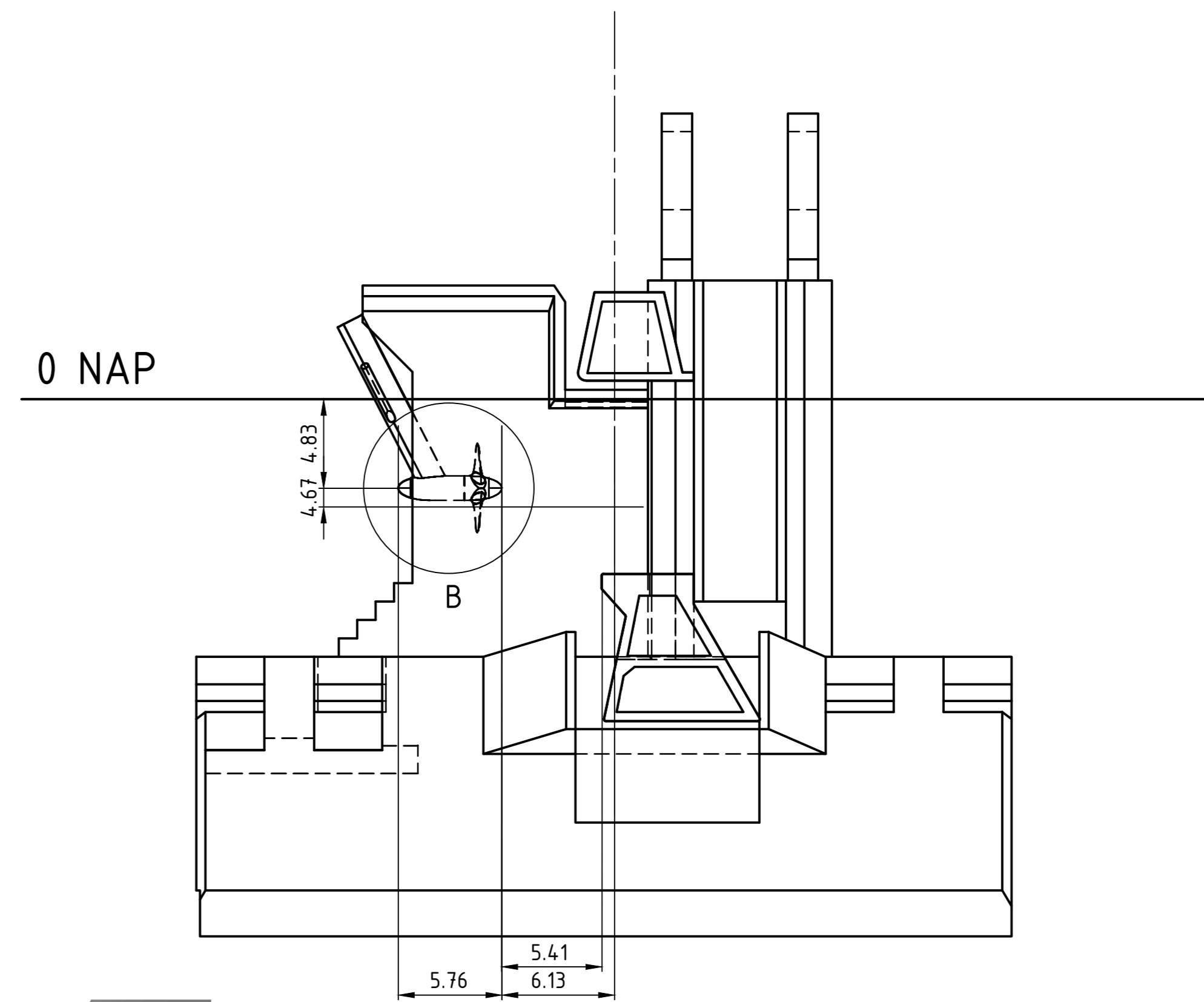
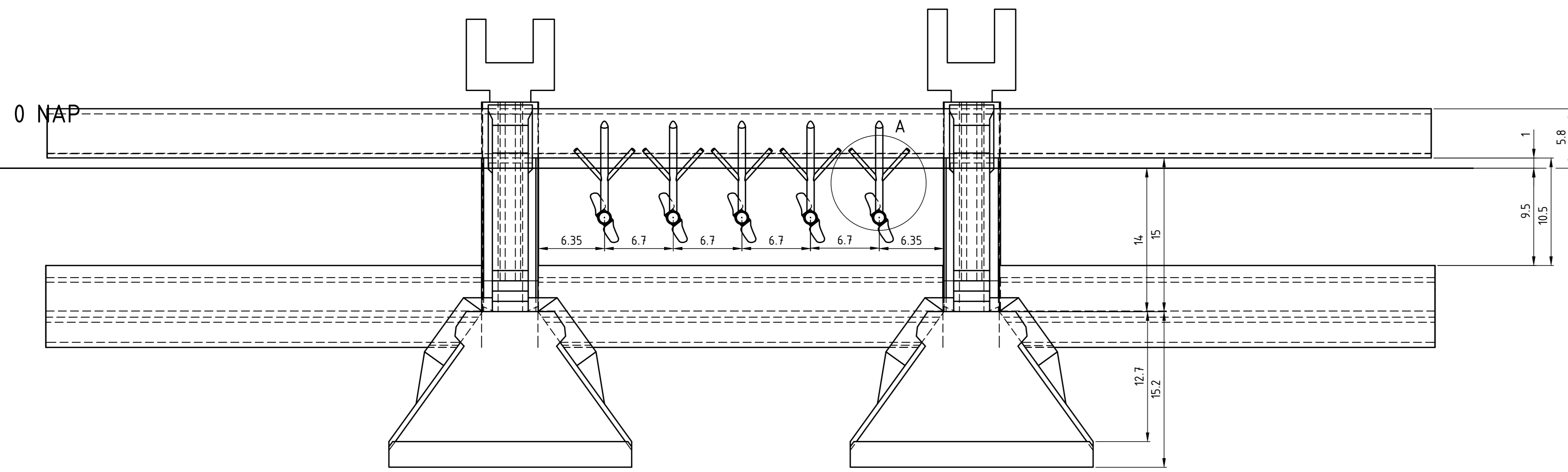
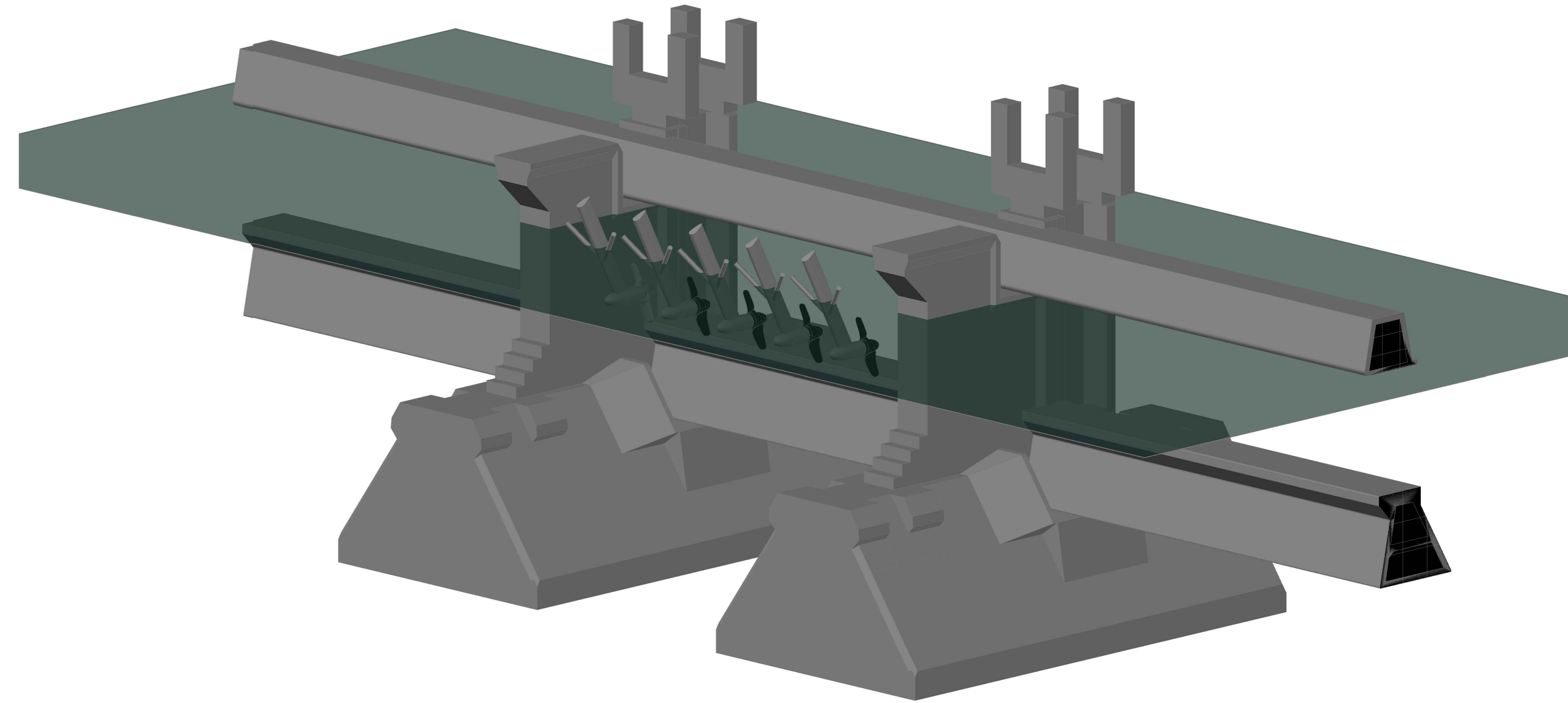
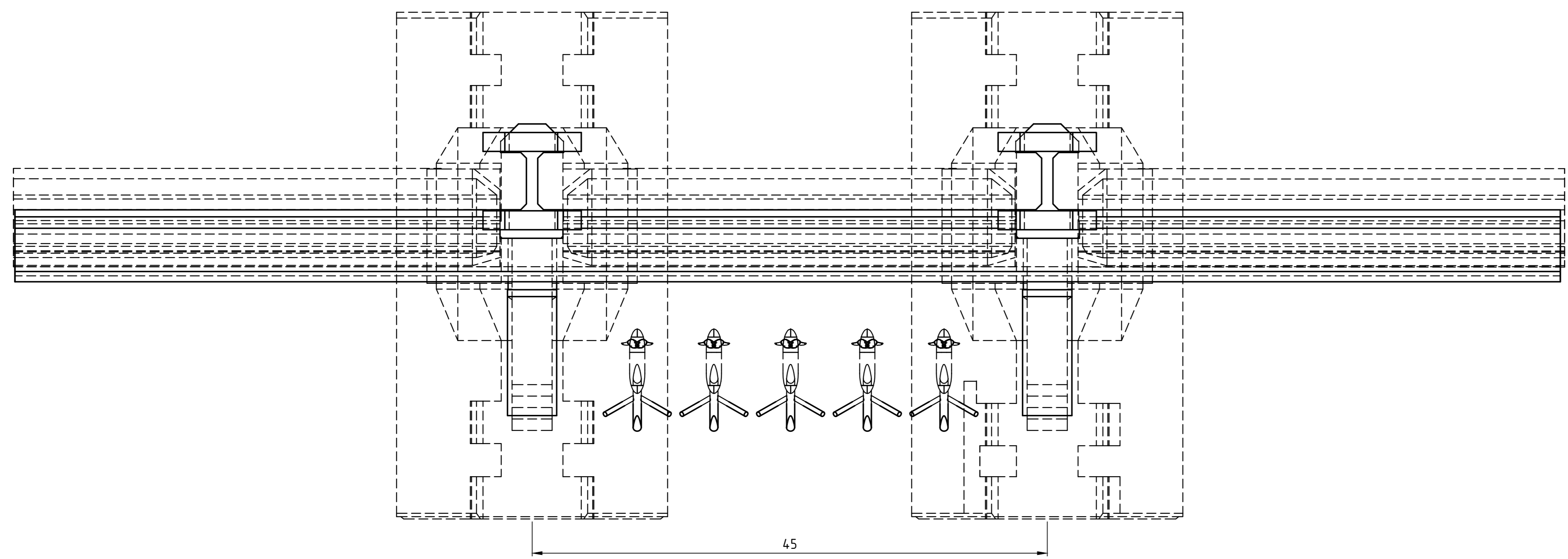
Detail C

1	7-jun-17		J.W.G. Ooms
Revise	Revised date	Description	Name
1		11200119-001_01	
Filename:	11200119-001_01	Material:	
Title:	Oosterschelde Roompot 8	Projectname:	DMET
			Sheet
			1 / 3
Drawn:	J.W.G. Ooms	Scale:	1 : 100
Checked:	A. Wijdeveld	Date:	6 maart 2017
Approved:	A. de Fockert	Project:	11200119-001

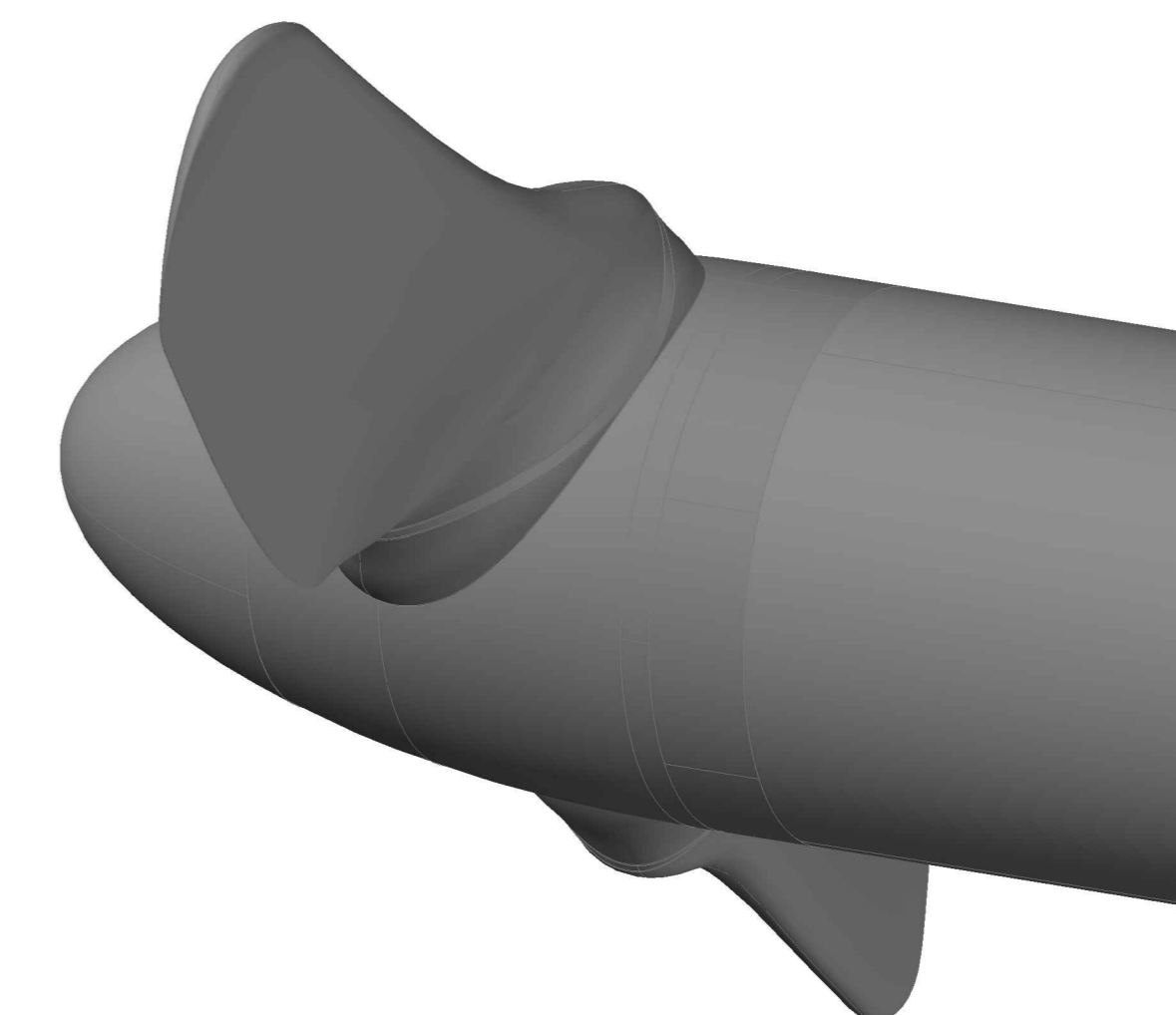


Control of this document, and that it is correct and that the use of it is limited to the project for which it was prepared, is the responsibility of the client.

Drawingno:	1120019-001_02	Material:	
Filename:		Projectname:	DMET
Title:	Aansluiting bodem bij Roompot 8		American Projection
			Sheet 2 / 3
		Drawn:	J.W.G. Ooms
		Checked:	A. Wijdeveld
		Approved:	A. de Fockert
		Scale:	1 : 100
		Date:	6 maart 2017
		Project:	1120019-001
			A0



Flood



Ebb

2	26-jun-11	Bemating ADCP	J.W.G. Ooms
1	7-jun-17		J.W.G. Ooms
Revise	Revisiedate	Description	Name
Drawing:	11200119-001_03	Material:	
Filename:		Projectname:	DMEC
Title:		American Projection:	3 / 3
Positie Turbines in Roompot 8			
Deltares		Drawn: J.W.G. Ooms	Scale: 1 : 100
Fronting Delta Ltd		Checked: A. Wijdeveld	Date: 6 maart 2017
		Approved: A. de Fockert	Project: 11200119-001

B Velocity profiles without turbines

B.1 Horizontal ADCP validation

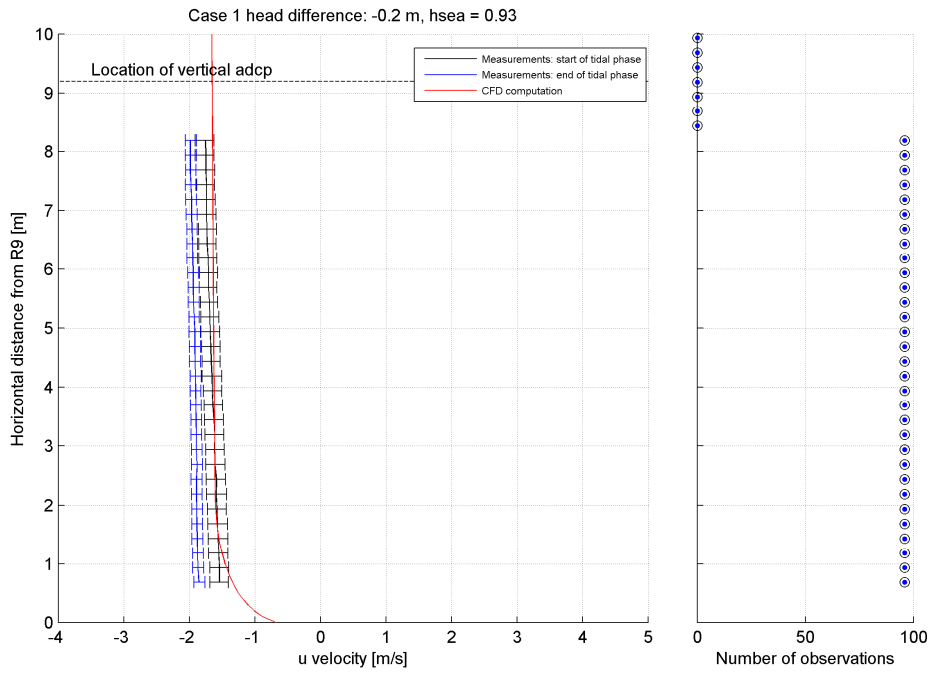


Figure B.1 Horizontal ADCP profile from the measurements without turbines – comparison between CFD and measurements – Ebb Case NT.1

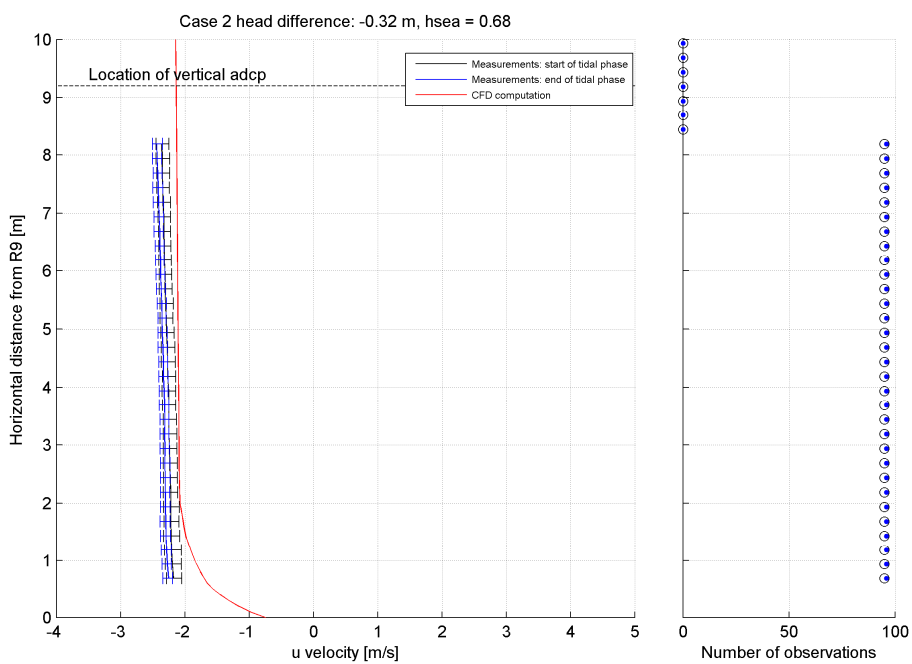


Figure B.2 Horizontal ADCP profile from the measurements without turbines – comparison between CFD and measurements – Ebb Case NT.2

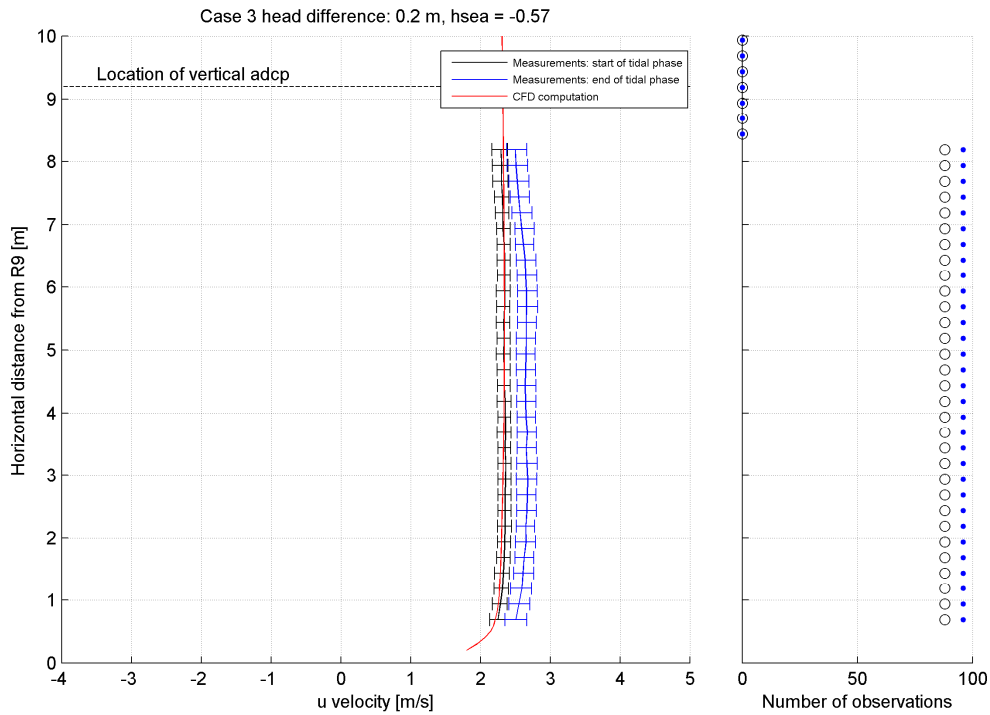


Figure B.3 Horizontal ADCP profile from the measurements without turbines – comparison between CFD and measurements – Ebb Case NT.3

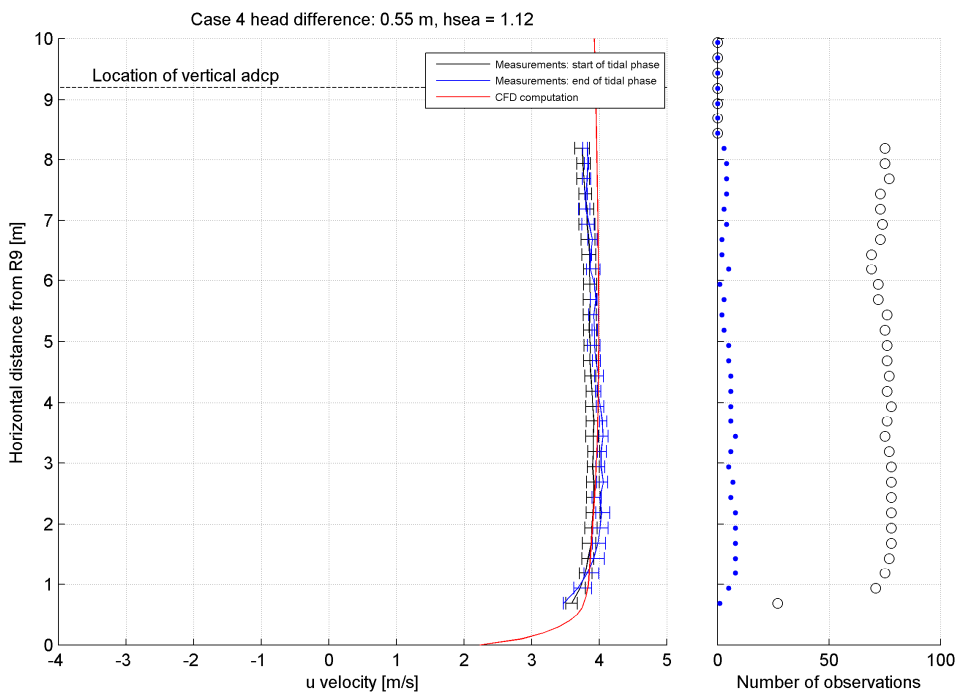


Figure B.4 Horizontal ADCP profile from the measurements without turbines – comparison between CFD and measurements – Ebb Case NT.4

B.2 Vertical ADCP validation

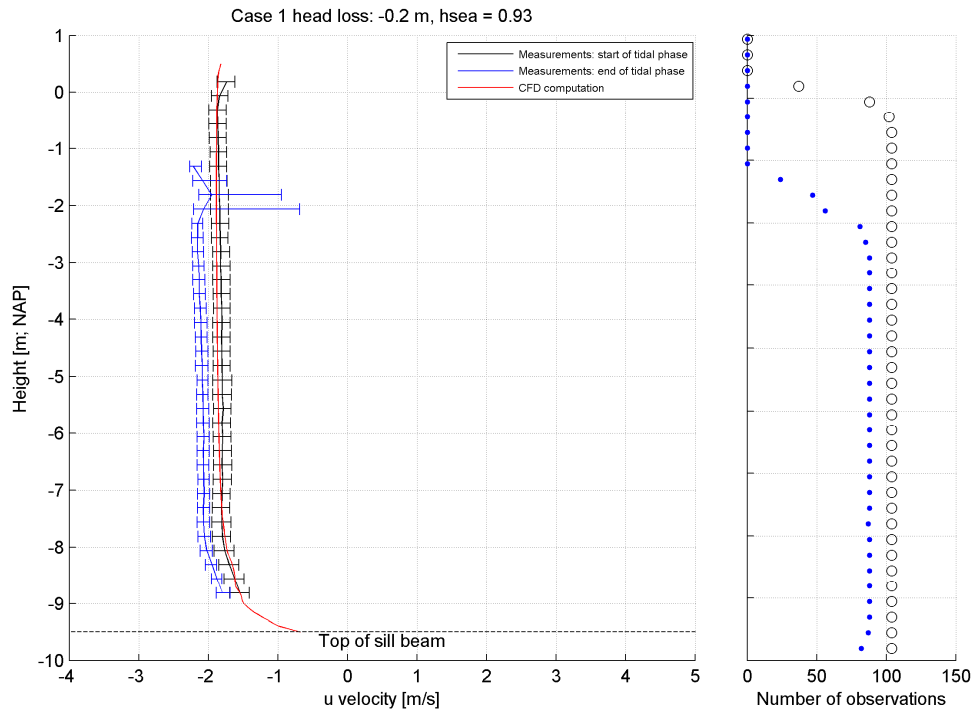


Figure B.5 Vertical ADCP profile from the measurements without turbines – comparison between CFD and measurements – Ebb Case NT.1

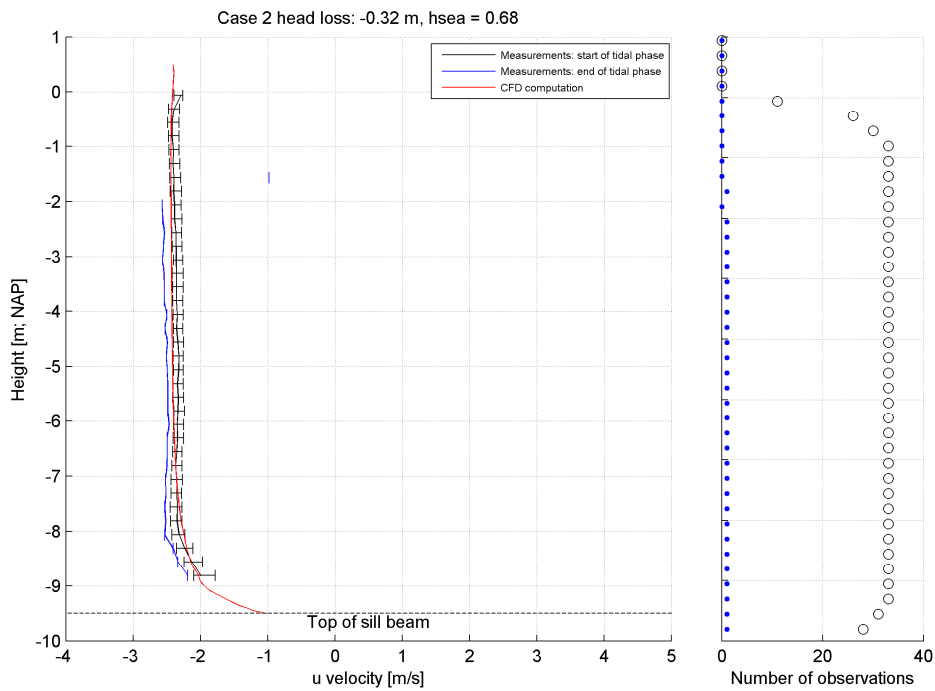


Figure B.6 Vertical ADCP profile from the measurements without turbines – comparison between CFD and measurements – Ebb Case NT.2

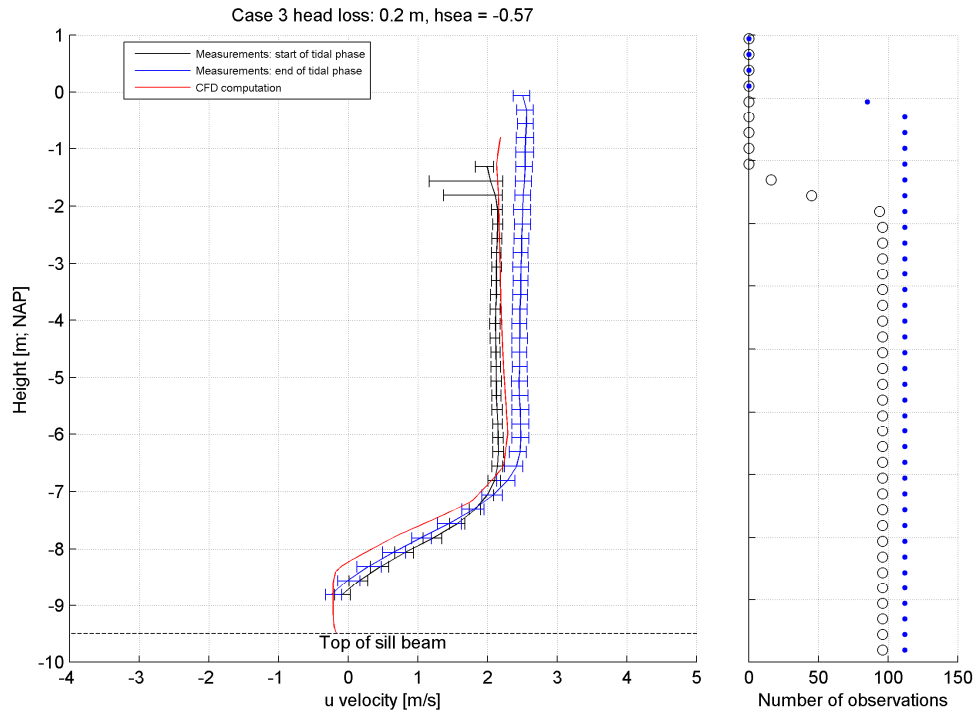


Figure B.7 Vertical ADCP profile from the measurements without turbines – comparison between CFD and measurements – Ebb Case NT.3

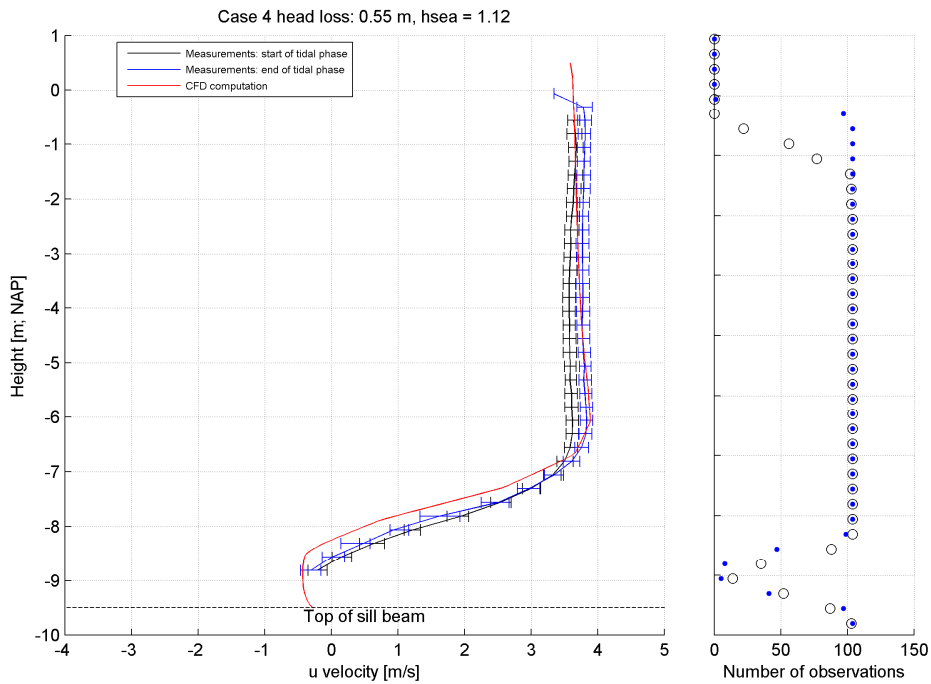


Figure B.8 Vertical ADCP profile from the measurements without turbines – comparison between CFD and measurements – Ebb Case NT.4

C Velocity profiles with turbines

C.1 Case 1 (head difference = -0.2m)

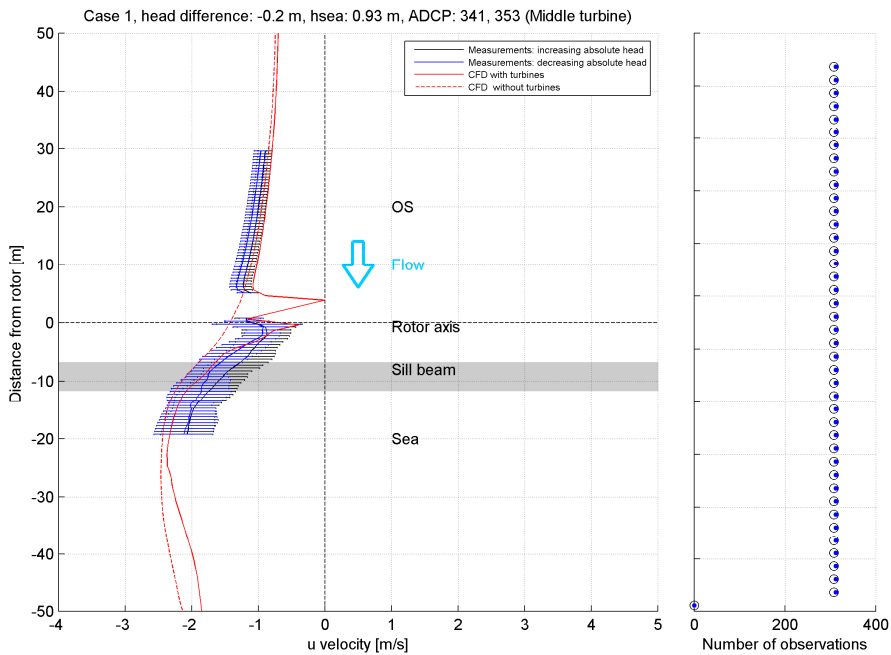


Figure C.1 Longitudinal ADCP profile from the measurements with turbines – comparison between CFD and measurements – Ebb Case WT.1. For illustrative purposes, the profile along the same line is also plotted for the corresponding simulation without turbines NT.1

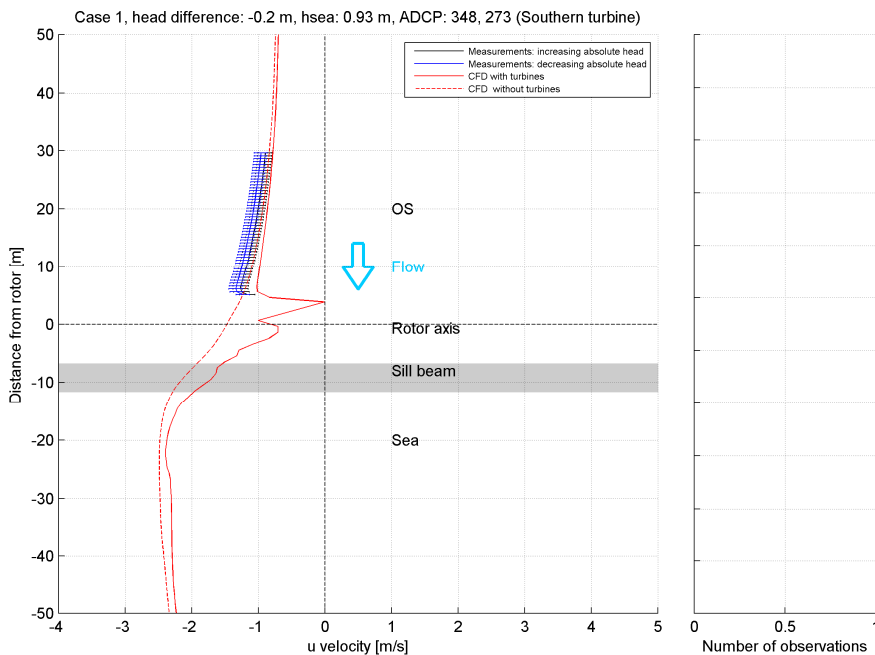


Figure C.2 Longitudinal ADCP profile from the measurements with turbines – comparison between CFD and measurements – Ebb Case WT.1. For illustrative purposes, the profile along the same line is also plotted for the corresponding simulation without turbines NT.1

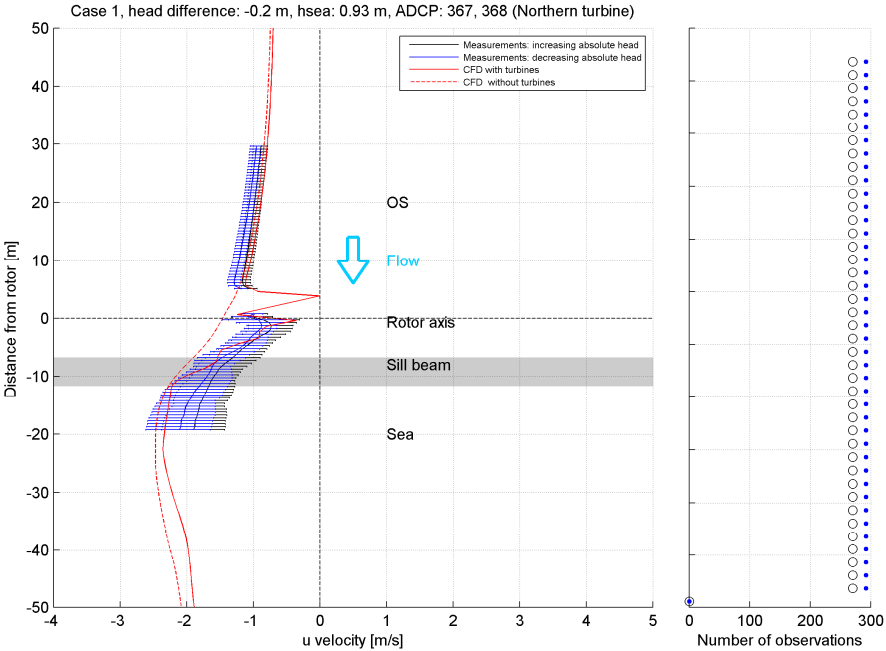


Figure C.3 Longitudinal ADCP profile from the measurements with turbines – comparison between CFD and measurements – Ebb Case WT.1. For illustrative purposes, the profile along the same line is also plotted for the corresponding simulation without turbines NT.1

C.2 Case 2 (head difference = -0.32m)

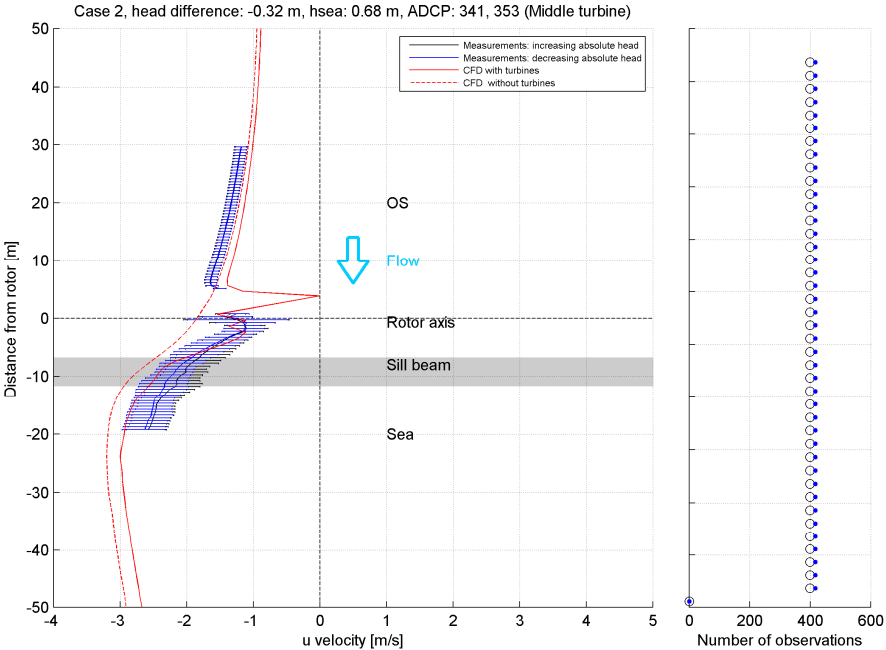


Figure C.4 Longitudinal ADCP profile from the measurements with turbines – comparison between CFD and measurements – Ebb Case WT.2. For illustrative purposes, the profile along the same line is also plotted for the corresponding simulation without turbines NT.2

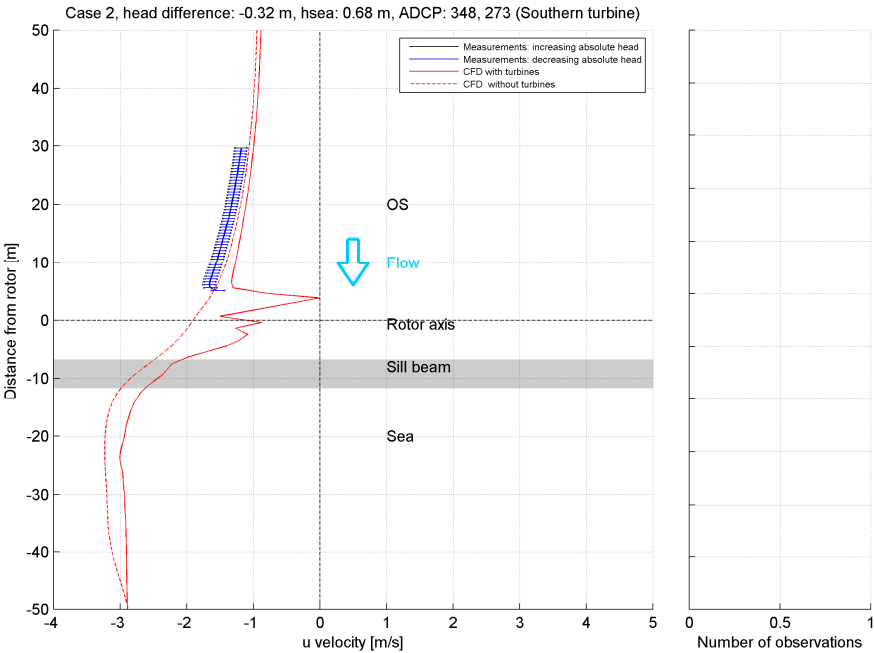


Figure C.5 Longitudinal ADCP profile from the measurements with turbines – comparison between CFD and measurements – Ebb Case WT.2. For illustrative purposes, the profile along the same line is also plotted for the corresponding simulation without turbines NT.2

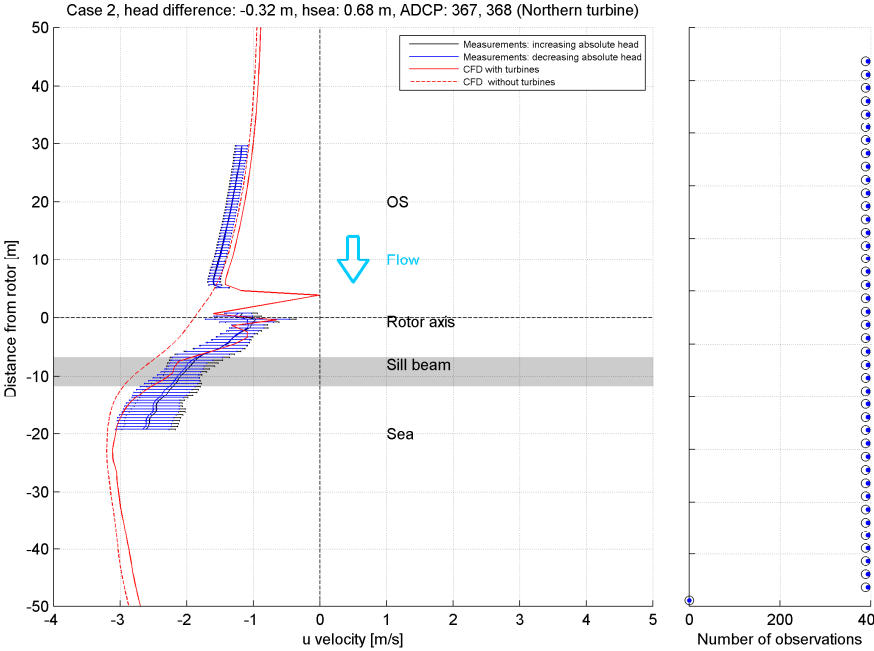


Figure C.6 Longitudinal ADCP profile from the measurements with turbines – comparison between CFD and measurements – Ebb Case WT.2. For illustrative purposes, the profile along the same line is also plotted for the corresponding simulation without turbines NT.2

C.3 Case 3 (head difference = +0.2m)

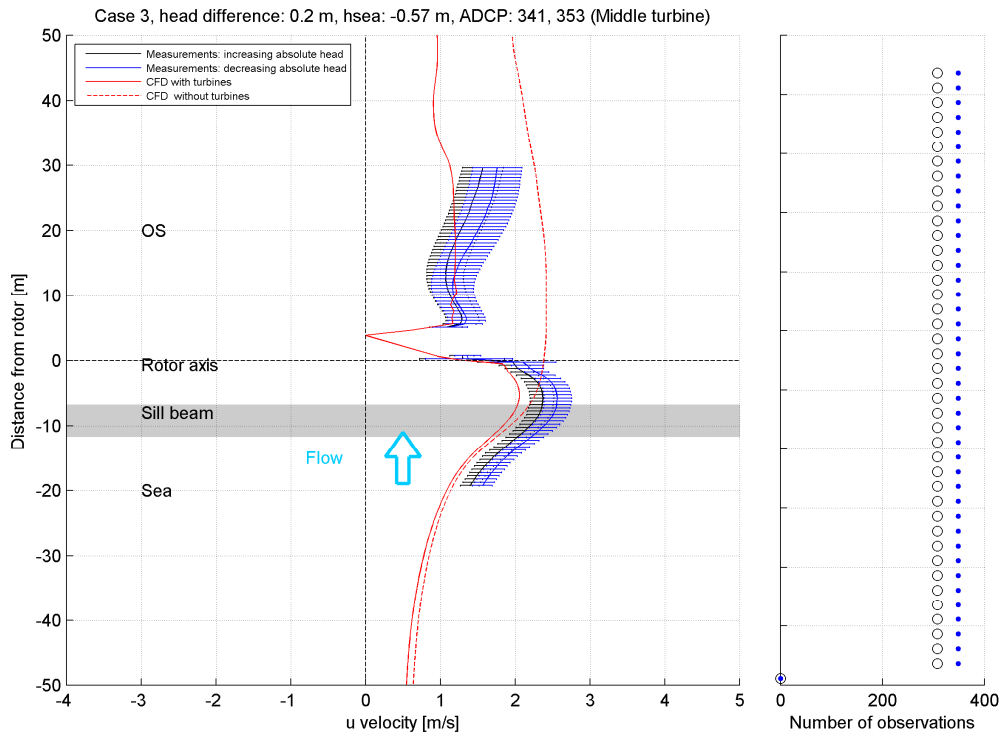


Figure C.7 Longitudinal ADCP profile from the measurements with turbines – comparison between CFD and measurements – Ebb Case WT.3. For illustrative purposes, the profile along the same line is also plotted for the corresponding simulation without turbines NT.3

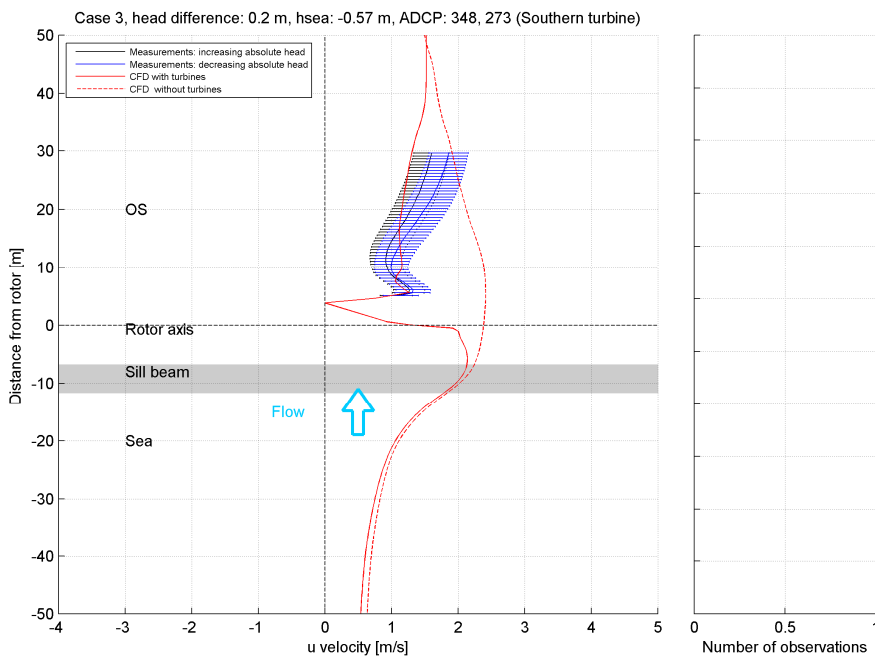


Figure C.8 Longitudinal ADCP profile from the measurements with turbines – comparison between CFD and measurements – Ebb Case WT.3. For illustrative purposes, the profile along the same line is also plotted for the corresponding simulation without turbines NT.3

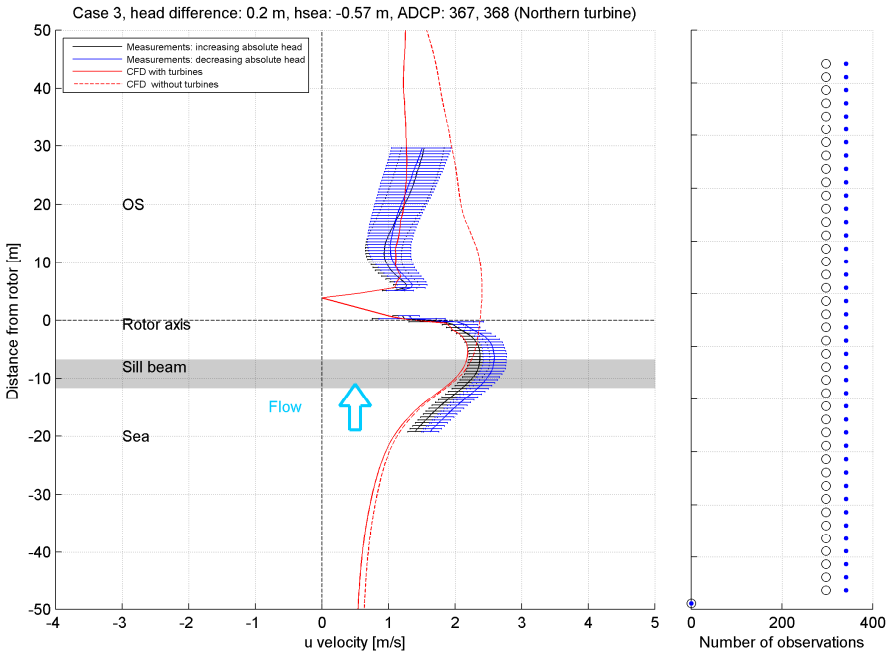


Figure C.9 Longitudinal ADCP profile from the measurements with turbines – comparison between CFD and measurements – Ebb Case WT.3. For illustrative purposes, the profile along the same line is also plotted for the corresponding simulation without turbines NT.3

C.4 Case 4 (head difference = +0.55m)

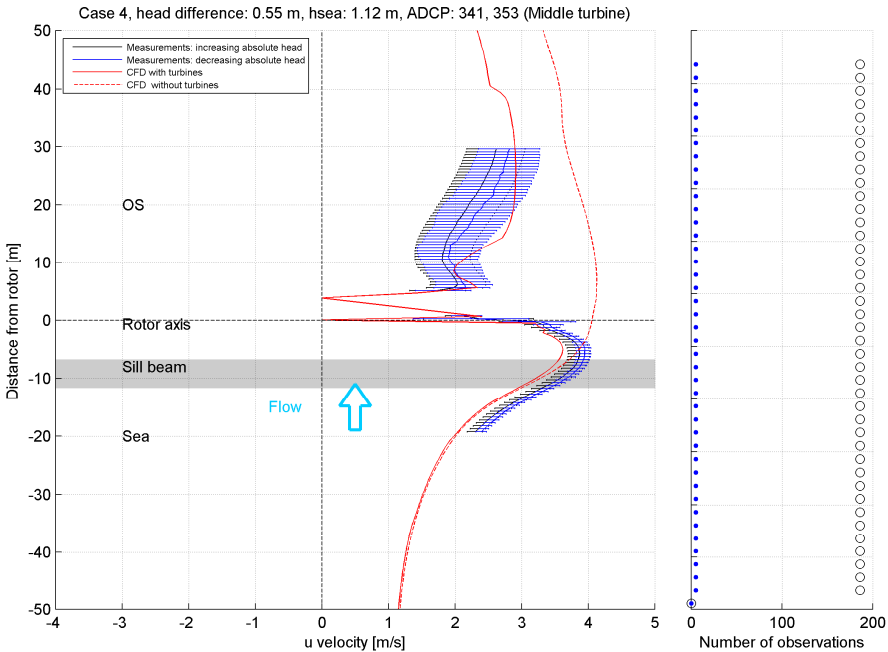


Figure C.10 Longitudinal ADCP profile from the measurements with turbines – comparison between CFD and measurements – Ebb Case WT.4. For illustrative purposes, the profile along the same line is also plotted for the corresponding simulation without turbines NT.4

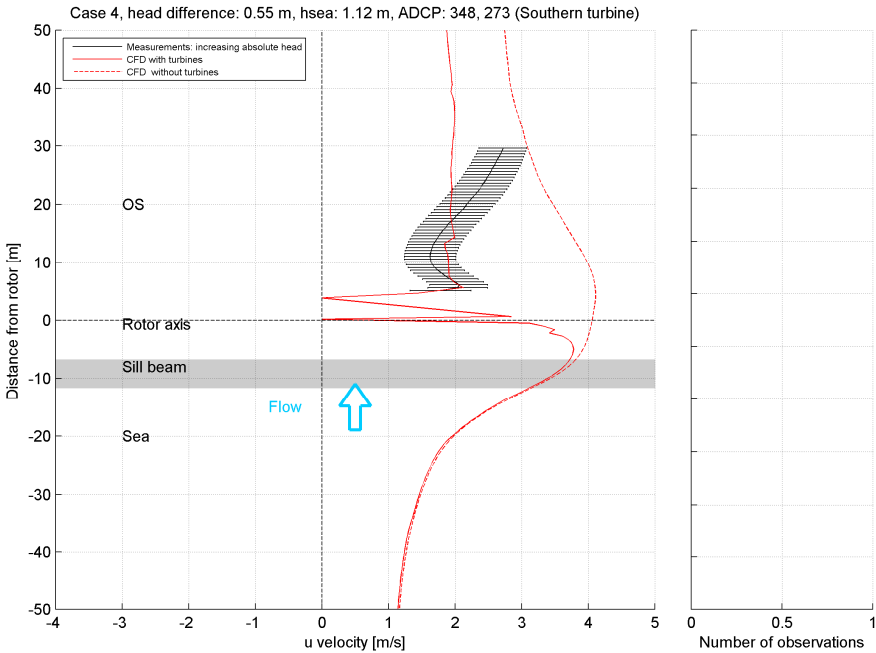


Figure C.11 Longitudinal ADCP profile from the measurements with turbines – comparison between CFD and measurements – Ebb Case WT.4. For illustrative purposes, the profile along the same line is also plotted for the corresponding simulation without turbines NT.4

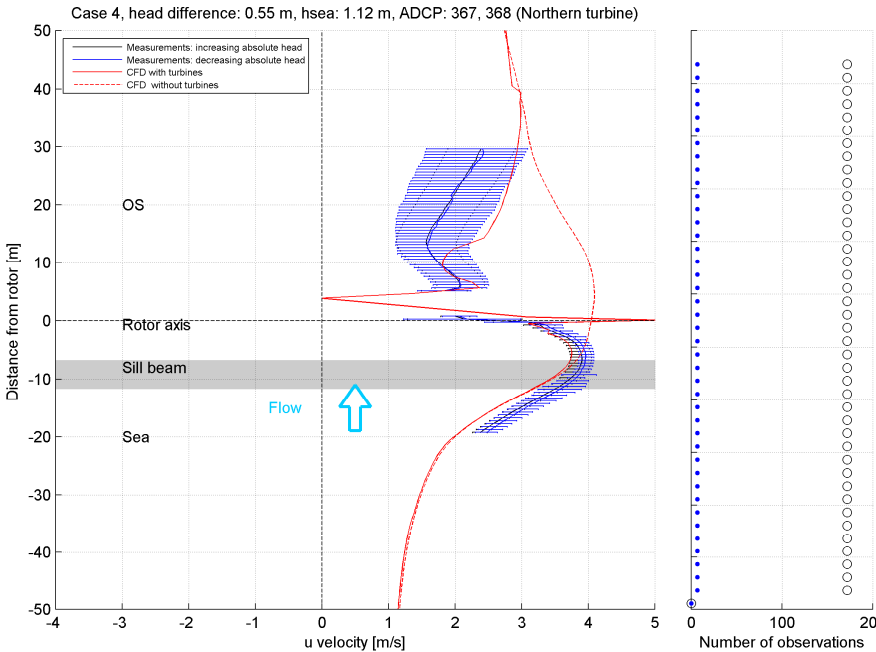


Figure C.12 Longitudinal ADCP profile from the measurements with turbines – comparison between CFD and measurements – Ebb Case WT.4. For illustrative purposes, the profile along the same line is also plotted for the corresponding simulation without turbines NT.4

